Author Manuscript

Author Manuscript

Author Manuscript

Author Manuscript

HHS Public Access

Author manuscript

Immunity. Author manuscript; available in PMC 2024 June 13.

Published in final edited form as:

Immunity. 2023 June 13; 56(6): 1303–1319.e5. doi:10.1016/j.immuni.2023.05.005.

Canonical BAF complex activity shapes the enhancer landscape that licenses CD8+ T cell effector and memory fates

Bryan McDonald[1,3,7], **Brent Y. Chick**[2,4,7], **Nasiha S. Ahmed**[2], **Mannix Burns**[2], **Shixin Ma**[1], **Eduardo Casillas**[1], **Dan Chen**[1], **Thomas H. Mann**[1], **Carolyn O' Connor**[5], **Nasun Hah**[6], **Diana C. Hargreaves**[2,*], **Susan M. Kaech**[1,8,*]

[1]NOMIS Center for Immunobiology and Microbial Pathogenesis, Salk Institute for Biological Studies, La Jolla, CA 92037, USA

[2]Molecular and Cell Biology Laboratory, Salk Institute for Biological Studies, La Jolla, CA 92037, USA

[3]Biomedical Sciences Graduate Program, University of California San Diego, La Jolla, CA 92093, USA

[4]Biological Sciences Graduate Program, University of California at San Diego, La Jolla, California 92093, USA.

[5]Flow Cytometry Core, The Salk Institute for Biological Studies, La Jolla, CA, USA

[6]Chapman Charitable Foundations Genomic Sequencing Core, The Salk Institute for Biological Studies, La Jolla, CA, USA

[7]These authors contributed equally

[8]Lead contact

Summary

CD8+ T cells provide host protection against pathogens by differentiating into distinct effector and memory cell subsets, but how chromatin is site-specifically remodeled during their differentiation is unclear. Due to its critical role in regulating chromatin and enhancer accessibility through its nucleosome remodeling activities, we investigated the role of the canonical BAF (cBAF) chromatin remodeling complex in antiviral CD8+ T cells during infection. ARID1A, a subunit

*Correspondence: Diana C. Hargreaves (dhargreaves@salk.edu) and Susan M. Kaech (skaech@salk.edu).
Contact Info
Susan M. Kaech
Director, NOMIS Center for Immunobiology and Microbial Pathogenesis,
Salk Institute for Biological Studies, USA

Author Contributions

Conceptualization, B.M., B.Y.C., D.C.H., S.M.K.; Methodology, B.M., B.Y.C.; Formal Analysis, B.M., B.Y.C., N.A.; Investigation, B.M., B.Y.C., N.A., M.B., S.M., E.C., D.C., T.M.; Resources, C.O., N.H.; Writing – Original Draft, B.M.; Writing – Review & Editing, B.M., D.C.H., S.M.K.; Funding Acquisition, D.C.H., S.M.K.; Supervision, D.C.H., S.M.K.

Publisher's Disclaimer: This is a PDF file of an unedited manuscript that has been accepted for publication. As a service to our customers we are providing this early version of the manuscript. The manuscript will undergo copyediting, typesetting, and review of the resulting proof before it is published in its final form. Please note that during the production process errors may be discovered which could affect the content, and all legal disclaimers that apply to the journal pertain.

Declaration of Interests

S.M.K. is on the scientific advisory boards and has equity in EvolveImmune Therapeutics, Affini-T Therapeutics, Arvinas, and Pfizer.

Author Manuscript Author Manuscript Author Manuscript Author Manuscript

of cBAF, was recruited early after activation and established *de novo* open chromatin regions at enhancers. *Arid1a* deficiency impaired the opening of thousands of activation-induced enhancers, leading to loss of TF binding, dysregulated proliferation, gene expression, and failure to undergo terminal effector differentiation. While *Arid1a* was dispensable for circulating memory cell formation, tissue-resident memory formation was strongly impaired. Thus, cBAF governs the enhancer landscape of activated $CD8^+$ T cells that orchestrates TF recruitment and activity and the acquisition of specific effector and memory differentiation states.

eTOC Blurb

Chromatin remodeling is a critical step for cellular differentiation. McDonald, Chick et al. show that the canonical BAF complex mediates chromatin remodeling to establish *de novo* enhancers in recently activated virus-specific $CD8^+$ T cells, which in turn allows the activated cells to acquire specialized effector and memory cell fates.

Graphical Abstract

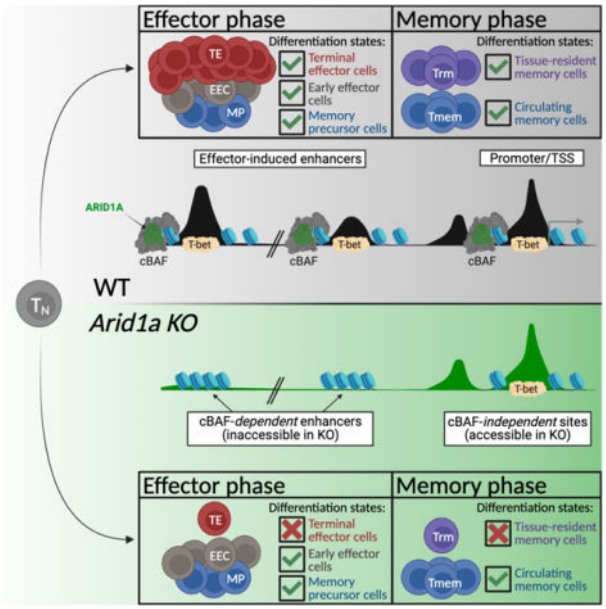

Keywords

Antiviral immunity; ARID1A; BAF Complex; Chromatin Remodeling; Epigenetics; CD8+ T cells; effector T cell; memory T cell; immunotherapy

Introduction

$CD8^+$ T cells play an essential role in host protection against intracellular pathogens and cancer. Naive $CD8^+$ T cells become activated upon recognition of cognate antigen (signal 1) concurrent with engagement of costimulatory receptors (signal 2) and cytokine signaling (signal 3), enabling epigenetic and transcriptional reprogramming to promote cell growth, proliferation, and the acquisition of specialized effector functions[1]. Activated effector

Author Manuscript Author Manuscript Author Manuscript Author Manuscript

cells exhibit transcriptional and epigenetic heterogeneity, display diverse modes of tissue homing patterns and memory-forming potential, and can be distinguished by expression of markers like IL7R (CD127), KLRG1 and CX_3CR_1[2]. Memory precursor (MP) cells express higher levels of CD127 and preferentially give rise to the long-lived circulating memory cell pool[3]. High inflammatory conditions promote the formation of short-lived terminal effector (TE) cells expressing KLRG1 and CX_3CR_1 that exhibit potent cytotoxic potential but preferentially die following the resolution of infection[4–6]. Early effector cells (EEC) express low levels of CD127, KLRG1, and CX_3CR_1, and can give rise to both TE and MP cells[6–8]. Recent studies have begun to identify distinguishing features of effector cells that preferentially migrate into non-lymphoid tissues to form tissue-resident memory (Trm) cells[9,10]. Importantly, while the identities of transcription factors (TFs) that promote effector (*Id2*, *Tbx21* (T-bet), *Batf*), tissue-residency (*Runx3*, *Zfp683*, *Bhlhe40*), and memory cell fates (*Eomes*, *Tcf7*, *Id3*, *Myb*) are well described[1,10–13], the underlying biological processes that regulate the binding and activity of these TFs are largely undefined. Indeed, individual TFs exert overlapping and distinct roles across many cell states (e.g., *Tbx21* and *Eomes* in memory versus exhausted T cells[14]) highlighting the need to better understand how TF binding site accessibility is regulated to control the behavior of TFs and the differentiation states they specify.

Mammalian SWI/SNF complexes (aka BAF, BRG/BRM-associated factors) are chromatin remodelers that facilitate reorganization of nucleosomes along DNA[15]. There are three variants: canonical BAF (cBAF), Polybromo-associated BAF (PBAF), and non-canonical BAF (ncBAF), each composed of many shared subunits, but distinguishable by inclusion of unique subunits, including ARID1A/ARID1B (cBAF), PBRM1/ARID2/BRD7 (PBAF), and GLTSCR1/GLTSCR1L/BRD9 (ncBAF)[16–18]. Enhancer accessibility is particularly sensitive to the loss of ARID1A, a key subunit of the cBAF complex[19–21]. Normal leukocyte development is accompanied by substantial chromatin remodeling and establishment of novel enhancers; and deletion of either *Arid1a* or *Smarca4* during murine hematopoiesis eliminates the formation of essentially all leukocyte lineages[22–24]. ARID1A mutations lead to dysregulated gene expression and differentiation patterns and are commonly found in human cancers[25,26], including T cell lymphomas[26–28]. However, it is unknown what role ARID1A plays in differentiating mature T lymphocytes and the generation of $CD8^+$ T cell memory. Given the importance of cBAF in regulating cellular differentiation in diverse contexts, we reasoned that cBAF could play a critical role in regulating the differentiation and functional diversification of activated T lymphocytes, a process that involves extensive chromatin remodeling[29,30].

Here we investigated the role of ARID1A-containing cBAF in promoting $CD8^+$ T cell effector differentiation upon acute systemic viral infection. We found that ARID1A was necessary for terminal effector cell differentiation and establishment of long-lived Trm cell populations but was dispensable for circulating memory cell formation. However, *Arid1a*-deficient circulating memory cells were deficient in production of cytokines, chemokines, and cytotoxic proteins, suggesting that ARID1A was critical for optimizing the functional capabilities of memory cells. Mechanistically, ARID1A was required to induce early expression of TFs that specify TE and Trm fates, as well as to open chromatin at sites where those TFs bind. *Arid1a*-deficient effector cells displayed reduced global chromatin

Author Manuscript Author Manuscript Author Manuscript Author Manuscript

accessibility and failed to open chromatin regions containing binding sites for ETS, RUNX, bZIP (AP-1), and T-box family transcription factors. Our results demonstrate that ARID1A-containing cBAF complexes act to remodel chromatin that licenses effector differentiation during acute infections and provide insight into how TF recruitment and activity is regulated to instruct the formation of different types of effector and memory $CD8^+$ T cells.

Results

Differentiating antiviral effector $CD8^+$ T cells display highly dynamic accessible chromatin and cBAF occupancy patterns

To better understand the initial waves of $CD8^+$ T cell differentiation during infection, we transferred P14 TCR transgenic cells that recognize the $GP_{33–41}$ epitope of the LCMV glycoprotein[31] into wild-type recipients infected with LCMV-Armstrong, and on days 3 (d3), 5 (d5), and 8 (d8) post-infection (p.i.) we mapped the changes in open chromatin regions (OCRs) and ARID1A binding sites in donor P14 cells using Assay for Transposase-Accessible Chromatin sequencing (ATAC-seq)[32] and CUT&RUN[33], respectively. In parallel, to assess even earlier changes we performed ATAC-seq on 48-hour *in vitro* activated P14 cells. We defined 5 OCR clusters corresponding to regions that are unique or conserved across differentiation timespace: (1) **Conserved-** OCRs conserved at all timepoints (n=21650), (2) **Naive-** OCRs unique to naive T cells (n=3157), (3) **Early Activation-** OCRs more selectively found at day 3 p.i. *in vivo* or 48h post-activation *in vitro* (n=7883), (4) **Activation-** OCRs open in all activated cells (n=8781), or (5) **Late Activation-** OCRs predominantly found at day 5 and day 8 p.i. *in vivo* effector timepoints (n=1250) (Figures 1A–C). ARID1A binding was highly enriched at OCRs and correlated with the dynamics of open chromatin across the time course of activation (Figures 1A, D; Figure S1A). Cluster annotations revealed that nearly half of Conserved sites align to promoters, while OCRs that were either lost or gained during activation were more frequently found at intergenic and intronic regions (Figure 1C). Consistent with the notion that enhancer rather than promoter accessibility patterns are the predominant determinants of cellular states[34], OCRs that opened and closed upon $CD8^+$ T cell activation were predominantly found in enhancers as defined by H3K4me1, H3K27ac[35], while promoter-specific H3K4me3 was more strongly enriched at Conserved OCRs than activation-induced OCRs (Figure 1E). In general, regions with increased chromatin accessibility annotated to genes with increased gene expression and vice versa whereas regions with unchanging chromatin accessibility exhibited little changes in gene expression (Figure S1B).

TF motif analysis on the five OCR clusters revealed a specific enrichment of HMG motifs (TCF, LEF) in Naive OCRs, while AP-1 (bZIP) motifs were enriched in Early and general Activation OCRs, and the nuclear receptor (NR) and T-box motifs were enriched in the Activation and Late Activation OCRs (Figure 1F; Figure S1C). Next, we overlapped physical TF binding patterns from naive, *in vitro* activated[36,37], and *in vivo* day 7 $CD8^+$ effector cells[38] with our peak clusters (Figure 1G). TF binding of ETS1, TCF1 and RUNX1 in naive cells was primarily restricted to Conserved and Naive OCRs with some binding in Late Activation OCRs, while binding of most TFs including BATF, IRF4, and T-bet strongly overlapped with Early Activation (*in vitro* activated cells) and Activation (*in vitro*

Author Manuscript Author Manuscript Author Manuscript Author Manuscript

activated and *in vivo* d7 cells) induced OCRs. Together, these data outline the temporal kinetics of newly formed enhancers in differentiating virus-specific CD8$^+$ T effector cells and demonstrate that these sites are associated with ARID1A-containing cBAF complexes and distinct sets of TFs at different phases of effector cell differentiation. These findings imply that the cBAF complex plays a central role in shaping the chromatin accessibility landscape and differentiation process in antiviral effector CD8$^+$ T cells.

Arid1a promotes clonal expansion and opening of activation-induced enhancers

To elucidate the function of ARID1A-containing cBAF in activated CD8$^+$ cells while avoiding developmental defects seen with early T cell *Arid1a* deletions[22,24], we crossed *Arid1a*$^{fl/fl}$ mice with *Gzmb-Cre*$^+$ mice (in which Cre is conditionally active after T cell activation) with *Arid1a*$^{fl/fl}$ mice to generate *Gzmb-Cre*$^+$ *Arid1a*$^{fl/+}$ (*Arid1a*^{cKO}) and *Gzmb-Cre*$^+$ *Arid1a*$^{fl/+}$ (*Arid1a*^{cHet}) mice[39]. *Gzmb-Cre*$^-$ *Arid1a*$^{fl/fl}$ or *Gzmb-Cre*$^-$ *Arid1a*$^{fl/+}$ mice were used as wild-type (WT) littermate controls. We further crossed these mice with P14 TCR transgenic mice (*Arid1a*^{cKO} P14). We then transferred 25,000 wild-type (WT) or *Arid1a*^{cKO} P14 CD8$^+$ T cells into naive congenic recipient mice and infected those mice with LCMV-Armstrong to induce acute viral infection. We confirmed the loss of ARID1A protein in virus-specific CD8$^+$ T cells within 72h of activation *in vivo* using flow cytometry (Figure S2A).

Clonal expansion of *Arid1a*^{cKO} cells was slightly impaired (~3-fold) early during the expansion phase (day 5 p.i.) and more strongly impaired (~7-fold) at the peak of the effector response (day 8 p.i.) (Figure 2A). P14 CD8$^+$ T cells electroporated with Cas9 *Arid1a* sgRNA ribonucleoproteins (RNP) similarly expanded less robustly relative to control RNP electroporated cells (Figure S2B). In line with these findings, *Arid1a*^{cKO} cells proliferated slower relative to WT cells as observed using CellTrace violet staining at day 3 p.i. (Figure 2B). Deletion of *Arid1a* in endogenous effector CD8$^+$ T cells coincided with ~10X higher LCMV titers at day 5 p.i. compared to the *Arid1a*^{cHet} and WT mice (Figure S2C), but then titers were undetectable in all mice by d8 p.i. (data not shown). However, *Arid1a* deletion had little impact on the numbers of memory CD8$^+$ T cells that formed in the spleen 30–60 days p.i. (Figures 2A and S2B). Thus, there was a strong dependence on ARID1A for the initial effector cell expansion phase, but not for contraction and seeding of the circulating memory pool.

To interrogate how ARID1A-dependent cBAF complexes control chromatin remodeling and enhancer accessibility during CD8$^+$ T cell differentiation we performed ATAC-seq on WT, *Arid1a*^{cHet}, and *Arid1a*^{cKO} P14 cells at d3, d5, and d8 p.i. and assessed chromatin accessibility at the five OCR clusters defined in Figure 1A. As early as day 3 p.i. *Arid1a*^{cKO} cells exhibited defects in chromatin accessibility in ~30–40% (n=2020) of the OCRs in the Early and Activation clusters (Figures 2C–E). By days 5 and 8 p.i., the KO effector cells showed greater loss in ~40–60% (n=4766 (d5), 2789 (d8)) of the Activation and ~30–40% (n=435 (d5), 350 (d8)) of Late Activation OCRs (Figures 2C–E). Several of these OCRs map to activationinduced genes, including effector-associated TFs, *Bhlhe40*, *Tbx21* (T-bet),

Author Manuscript Author Manuscript Author Manuscript Author Manuscript

Zeb2, and *Batf* (Figure S2D). Sites with reduced accessibility in KO cells were also depleted of H3K27ac deposition indicating that cBAF promotes histone acetyltransferase activity at the enhancers it remodels (Figure 2F). In contrast, accessibility in Conserved OCRs was not affected by *Arid1a*-deficiency (Figures 2C–E), suggesting that although ARID1A was bound to these promoters and other sites (Figures 1A, D), it was not necessary for maintaining their accessibility. These data demonstrate that cBAF is necessary for the initial opening and/or maintenance of thousands of activation-induced enhancers created during effector $CD8^+$ T cell differentiation.

We next assessed transcriptional changes of d3 early effector WT and KO cells and identified 534 genes significantly lower and 595 genes higher in $Arid1a^{cKO}$ cells compared to WT cells (Figure 2G). Interestingly, $Arid1a^{cKO}$ cells are markedly deficient in the expression of several effector-associated TFs, including *Bhlhe40*, *Tbx21* (T-bet), *Zeb2*, and *Batf*, but expressed higher levels of naive-associated TFs like *Maf*, *Myb*, and *Tcf7* (Figure 2H). Gene set enrichment analysis (GSEA)[40] revealed a strong decrease in Hallmark MYC target genes in $Arid1a^{cKO}$ cells (Figure 2I), including *Myc*, *Srm*, and *Dusp2*, as well as other critical regulators of murine T lymphocyte function and cell growth, *Tfrc* (CD71) and *Slc7a5* (CD98) (Figure 2H)[41]. Additionally, several genes encoding cyclin-dependent kinase inhibitors including *Cdkn1b, Cdkn2d*, *Cdkn2a* were more highly expressed in $Arid1a^{cKO}$ cells, which together with decreased *Myc* expression may explain the reduced proliferative rate (Figure 2B). Overall, these data indicate that ARID1A acts early in $CD8^+$ T cell activation to establish OCRs at the enhancers of key T cell differentiation genes, including driver TFs. Failure to open these enhancers and achieve optimal gene expression leads to an overall dampening of early effector $CD8^+$ T cell expansion and differentiation and likely many downstream deficiencies in the activation of subsequent OCRs and late-stage effector differentiation programs.

Arid1a acts in a dose-dependent manner to specify effector subsets

To understand how cBAF regulates the formation of different specialized effector subtypes we first compared WT and $Arid1a^{cKO}$ effector cells at 8 days p.i. by flow cytometry and found that the $Arid1a^{cKO}$ cells contained very few $KLRG1^+$ and $CX3CR1^{hi}$ cells and were skewed towards a $CD127^{hi}$ MP-like phenotype[3] (Figures 3A–B), indicating that terminal effector differentiation was impaired but that cells retained similar potential to give rise to a long-lived circulating memory cell pool. Similar results were obtained in P14 cells in which *Arid1a* was deleted via Cas9 RNP as well as comparing WT and $Arid1a^{cKO}$ endogenous, polyclonal LCMV-specific effector $CD8^+$ T cells (Figures S3A–C). Between 5–20% of $KLRG1^+$ $CD127^{lo}$ TE cells, but not EEC or MP cells, retained ARID1A expression, suggesting the strict requirement for ARID1A for TE differentiation selects for Cre recombinase escapers (Figures S3D–E). $Arid1a^{cHet}$ cells displayed an intermediate TE/MP phenotype between that of WT and KO cells (Figures 3A–B), indicating that ARID1A acts in a dose-dependent manner to promote effector cell fates. $Arid1a^{cKO}$ effector cells mounted similar cytokine responses as WT cells after $GP_{33–41}$ peptide stimulation, but produced significantly less IFNγ after stimulation by IL-12 and IL-18 and expressed lower levels of granzyme A (Figures S3F–G). As T-bet is a critical inducer of TE cells[6,42], we measured T-bet expression (Figures 3C–D; Figure S3H) and observed ~50% lower T-bet

Author Manuscript Author Manuscript Author Manuscript Author Manuscript

protein in *Arid1a*^{cKO} cells compared to WT cells, consistent with a reduction in *Tbx21* transcripts at d3 (Figure 2H). Together, these results indicated that ARID1A-dependent cBAF is needed to permit the differentiation of TE cells, and in the absence of ARID1A, activated T cells fail to upregulate T-bet and preferentially acquired EEC- and MP-like differentiation states.

We next performed bulk RNA-seq on FACS-purified KLRG1^{+} CD127^{lo} (TE), KLRG1^{-} CD127^{lo} (EEC), and KLRG1^{-} CD127^{hi} (MP) subsets from WT, *Arid1a*^{cHet,} and *Arid1a*^{cKO} cells at d8 p.i. Principal component analysis (PCA) revealed that the majority of transcriptional variation was explained by the underlying donor cell genotype, and secondarily by subset, indicating that *Arid1a*^{cHet} and *Arid1a*^{cKO} subsets are transcriptionally distinct from their WT cell counterparts (Figures 3E–F). Differential gene expression analysis revealed that 446 TE, 779 EEC, and 986 MP genes were downregulated and 597 TE, 973 EEC, and 679 MP genes were upregulated in *Arid1a*^{cKO} cells relative to WT cells (Figure 3F). DEGs in *Arid1a*^{cHet} cells (downregulated: 61 TE, 151 EEC, 99 MP; upregulated: 75 TE, 150 EEC, 65 MP) were almost entirely a subset of those affected in *Arid1a*^{cKO} cells.

Across all effector subsets, *Arid1a*^{cKO} cells expressed lower levels of several TFs (*Tbx21*, *Zeb2*, *Eomes*, *Zfp683*, *Bhlhe40*), trafficking and adhesion molecules (*Cx3cr1*, *S1pr1, Itga1*, *Itga4*) and NK cell-associated genes (*Klrk1* (NKG2D), *Klrc1* (NKG2A)) relative to the WT cells (Figure 3G). Conversely, *Arid1a*^{cKO} cells expressed higher levels of TFs (*Irf4, Myb*, *Maf*, *Batf3*), chemokine receptors (*Ccr9, Ccr7, Ccr5*) and the cytokine *Il21*. In general, *Arid1a*^{cHet} cells had an intermediate gene expression phenotype between WT and *Arid1a*^{cKO} cells, except for a small number of genes (*Klrc2, Klra1, Klra4, Lrp6*) that exhibited ectopic expression in *Arid1a*^{cHet} cells, but not in *Arid1a*^{cKO} cells (Figure 3G). Additionally, *Cxcr3* gene expression and CXCR3 protein was reduced in *Arid1a*^{cHet} cells but increased in the *Arid1a*^{cKO} cells (Figures 3A, G). Analysis of TE- and MP-signature genes within the individual subsets showed that several TE-signature genes such as *Tbx21, S1pr5, Cx3cr1, Zeb2, GzmA,* and *Klrg1* were downregulated and several MP-signature genes like *Tcf7, Id3, Cxcr3* were upregulated in *Arid1a*^{cKO} KLRG1^{+} CD127^{lo} TE cells relative to WT TE cells (Figure 3H). Indeed, GSEA showed that *Arid1a*^{cKO} TE cells were enriched with a more MP-like transcriptional signature relative to WT TE cells (Figure 3I). The failure to activate TE-signature genes and repress MP-signature genes was also observed in the *Arid1a*^{cKO} KLRG1^{-} CD127^{lo} EECs (Figures 3G–H). Conversely, comparison of WT and *Arid1a*^{cKO} KLRG1^{-} CD127^{hi} cells revealed aberrant expression patterns of both MP- and TE-signature genes in *Arid1a*^{cKO} MP cells (Figures 3G–H). Specifically, *Arid1a*^{cKO} MP cells expressed higher levels of MP-signature genes like *Ccr7* and *Slamf6* and TE-signature genes like *Prdm1, Gzmk, GzmB* and *Ccr5*, but lower levels of other MP-signature genes like *Gzmm* and *Aqp9* (Figures 3G–H). In general, the *Arid1a*^{cKO} cells shared gene expression patterns similar to those observed in *Tbx21* KO[43] and *Runx3* KO CD8^{+} T cells[44] (Figure 3I). These data reveal that loss of *Arid1a* has profound effects on the ability of activated CD8^{+} T cells to properly engage canonical effector and memory gene expression programs and that *Arid1a* is haploinsufficient for the expression of many of these genes.

Author Manuscript Author Manuscript Author Manuscript Author Manuscript

Arid1a-dependent OCRs in d8 effector cells are largely shared across subsets

To better understand how *Arid1a* regulates gene expression and cell fate specification of $CD8^+$ T cells, we analyzed OCRs in TE, EEC and MP subsets from WT, $Arid1a^{cHet}$, and $Arid1a^{cKO}$ cells at d8 p.i. PCA revealed that the principal source of variation in global chromatin accessibility was dictated by donor cell genotype rather than subset (Figure 4A). Critically, comparison of differential OCRs between WT and $Arid1a^{cKO}$ subsets showed that nearly all differential OCRs lost accessibility in $Arid1a^{cKO}$ cells whereas only a fraction of sites gained accessibility (Figure 4B), indicating that the primary function of cBAF in activated $CD8^+$ T cells is to create and/or maintain OCRs through nucleosome remodeling. Analysis of $Arid1a^{cHet}$ cells showed a statistically significant loss (≥2-fold) of chromatin accessibility at ~1000 sites, all of which were also affected in $Arid1a^{cKO}$ cells, and essentially no gains (Figures 4B–C). Additionally, nearly every OCR significantly lost in $Arid1a^{cKO}$ cells displayed a substantial reduction in accessibility in the $Arid1a^{cHet}$ cells (Figure 4C), indicating that the level of accessibility is sensitive to the dosage of cBAF activity, which has clinical relevance to T cell lymphoma where *Arid1a* haploinsufficiency is commonly observed[27]. Next, we compared the differential OCRs between TE, EEC and MP subsets to see if loss of *Arid1a* affected one subset more than another. *Arid1a*-deficiency impaired the opening of 12,260 OCRs in TE cells, which helps to explain the lack of TE development in the $Arid1a^{cKO}$ cells, but surprisingly, even more OCRs (EEC n=16400, MP n=15110) were affected in the EEC- and MP-like subsets (Figures 4B, D). Further, of the OCRs lost in the $Arid1a^{cKO}$ d8 effector subsets, the majority were common to all three subsets (n=7802) whereas a minority were subset-specific (TE n=2169, EEC n=2843, MP n=2943) (Figure 4D). Together, these data demonstrate that although *Arid1a*-deficiency preferentially impaired the formation of $KLRG1^+$ TE cells, there was no biased requirement for cBAF activity in any one subset. Rather, all three subsets required cBAF to create thousands of enhancers both common to and uniquely found in each subset, and loss of cBAF activity resulted in aberrant gene expression patterns and differentiation states in all three subsets.

It is well established that accessibility of *cis*-regulatory elements strongly correlates with gene expression. Indeed, we found that many DEGs in EEC, TE and MP cells also lost OCR accessibility in the absence of ARID1A (Figure 4E). We focused on the expression of TE- and MP-signature genes within each subset and as predicted there was a strong requirement for *Arid1a* for both the accessibility and expression of TE- and MP-signature genes in all the subsets (although, by definition, the expression of TE-signature genes in MP cells was considerably lower than in TE cells and *vice versa* (see Figure 3G)). Most *Arid1a*-dependent OCRs that were annotated to genes downregulated in $Arid1a^{cKO}$ vs. WT cells had reduced H3K27ac, as exemplified by *Tbx21*, *Bhlhe40*, *Zfp683*, and *Prdm1* (Figures 4F; Figure S4A). Interestingly, we also observed loss of chromatin accessibility at sites annotated to genes that were upregulated in $Arid1a^{cKO}$ EEC, TE, and MP cells (Figure 4E, lower right quadrants), including many MP-signature genes. At such loci (e.g. *Sell*, *Ccr7*, *Cd9*, and *Tcf7*), H3K27me3 was reduced in $Arid1a^{cKO}$ EEC and TE cells suggesting that ARID1A promotes Polycomb-dependent silencing of MP-signature genes in these subsets (Figures S4B). Collectively, these data indicate that ARID1A is required in a dose-dependent manner to generate chromatin accessibility at shared and subset-specific OCRs induced during

Author Manuscript Author Manuscript Author Manuscript Author Manuscript

CD8$^+$ T cell differentiation. Failure to generate these accessible regions in *Arid1a*^{cKO} cells impairs their ability to properly activate 'proeffector' genes and regulate 'pro-memory' genes, perhaps due to a loss in the binding of TFs and epigenetic modifiers with activating and repressive regulatory properties at ARID1A-dependent accessible sites.

cBAF is required for targeting of T-bet to enhancers in effector CD8$^+$ T cells

To determine which TFs were most dependent on ARID1A activity, we performed TF motif enrichment on the ARID1A-dependent OCRs for each d8 effector subset. This revealed an enrichment of ETS, Runt, bZIP, T-box, and other TF family motifs, suggesting that binding sites for these factors may be less accessible in *Arid1a*-deficient effector cells, while CTCF motifs were enriched among gained sites (Figure 5A). In support of this, binding of FOSL2, EOMES, BATF, and T-bet[37] was selectively and highly enriched at ARID1A-dependent, but not ARID1A-independent OCRs (Figure 5B). To directly examine how certain TFs were affected by ARID1A deficiency we performed CUT&RUN on WT and *Arid1a*^{cKO} d5 effector cells against ETS1, BATF, and T-bet (representing ETS, bZIP, and T-box family members) and mapped their binding at ARID1A-dependent and -independent OCRs (Figure 5C). This showed a significant and strong reduction in ETS1, BATF, and T-bet binding at ARID1A-dependent OCRs, while ETS1 and BATF binding was less affected at ARID1A-independent OCRs. T-bet binding was universally affected genome-wide, likely because of both reduced T-box motif availability and reduced T-bet expression. The TF binding sites most affected by ARID1A-deficiency were predominantly found at intergenic and intronic sites (*i.e.*, enhancers), whereas those bound to ARID1A-independent sites were more frequently annotated to promoters (Figure 5C). These data demonstrate that cBAF-dependent remodeling is predominantly required in activated CD8$^+$ T cells to create enhancers that allow the binding of many key TFs that in turn, govern the gene regulatory networks controlling effector and memory CD8$^+$ T cell differentiation.

However, a potential caveat in the experiments above is that the defects in TF binding could stem from several alterations in the ARID1A-deficient cells including reduced expression of certain TFs. Therefore, to bypass some of these confounding issues we used a model of acute disruption of cBAF subunits in *in vitro* activated T cells with ACBI1[45], a PROTAC targeting BRG1, BRM, and PBRM1, or BRM014[46], an allosteric ATPase inhibitor of BRG1 and BRM. P14 CD8$^+$ T cells were activated *in vitro* for 48 hours and then treated with either DMSO or ACBI1/BRM014 for 4h prior to 2h treatment with IL-12 to enhance T-bet expression and binding, after which the cells were collected for T-bet ChIP-seq and ATAC-seq. This revealed that BAF complexes were required to maintain chromatin accessibility at ~7500 sites following BAF disruption (Figures 5D–E) and T-bet binding was selectively reduced at these sites. In contrast, T-bet binding was preserved or enhanced at BAF-independent OCRs (Figures 5D–E). Again, cBAF-dependent T-bet binding sites were almost universally annotated to intronic and intergenic elements, while cBAF-independent sites were more highly enriched for promoters (Figure 5F). These data indicate that ATP-dependent cBAF complex remodeling is acutely required to maintain T-bet binding at enhancers in activated CD8$^+$ T cells.

Author Manuscript Author Manuscript Author Manuscript Author Manuscript

To further assess how T-bet and cBAF may cooperate, we compared the OCRs between WT or *Tbx21* KO P14 CD8$^+$ T cells at d8 p.i. and found that *Tbx21*-deficiency resulted in reduced and gained accessibility at several thousand sites (Figure S5A). Notably, the majority of sites that lost accessibility in *Tbx21* KO cells also lost accessibility in *Arid1a*^{cKO} cells (n=2531, 90.4% (TE); n=3285, 76.1% (MP) (Figure 5G), and ARID1A binding was strongly reduced in *Tbx21* KO cells at these T-bet/ARID1A co- dependent OCRs (Figure 5H), strongly suggesting that T-bet engages ARID1A to promote accessibility at this subset of activation-induced OCRs. Finally, we tested if the requirement for cBAF to generate TE cells could be overridden by T-bet over-expression. To this end, we over-expressed T-bet in WT or *Arid1a*^{cKO} P14 cells and transferred them into mice infected with LCMV-Armstrong. Intriguingly, T-bet overexpression was unable to restore the ability of *Arid1a*^{cKO} cells to form TE cells (Figure 5I; Figure S5B), indicating that higher levels of T-bet are insufficient to compensate for the loss of cBAF activity due to decreased enhancer accessibility. Furthermore, while T-bet overexpression led to a significant enhancement of T-bet binding in WT cells, the stark inability of T-bet to bind chromatin in *Arid1a*^{cKO} cells was essentially unaltered by T-bet overexpression (Figure 5J), indicating that T-bet is completely reliant on ARID1A to make its binding sites accessible. Collectively, these data demonstrate that cBAF is critical for establishing and maintaining accessibility of thousands of enhancers and binding of several effector-associated TFs, particularly T-bet, in activated CD8$^+$ T cells. Further, while T-bet is necessary and sufficient to induce TE cell differentiation, this activity is entirely reliant on ARID1A.

Arid1a is critical for CD8$^+$ Trm formation

Our results demonstrated that similar numbers of WT and *Arid1a*^{cKO} memory CD8$^+$ T cells formed in the spleen following LCMV-Armstrong infection, yet the genetic and epigenetic analysis of MP-like cells revealed several alterations in the *Arid1a*^{cKO} cells. Therefore, to more broadly understand how *Arid1a* affected memory T cell development we computationally predicted the TFs most functionally impacted in MP cells by *Arid1a*-deficiency using the Taiji PageRank algorithm that assesses the global influence of TFs in a given cell state[47]. This analysis identified ZFP683, BHLHE40, RUNX3, RXRA and SMAD3 in addition to T-bet and EOMES as top-ranked TFs whose activity is predicted to be impaired in *Arid1a*^{cKO} MP cells (Figure 6A; Figure S6A). This was noteworthy because ZFP683, BHLHE40, and RUNX3 are critical to the formation of tissue-resident memory (Trm) cells[10,12,13] and indeed, MP cells required ARID1A for promoting expression of both *Zfp683* and *Bhlhe40*, as well as increasing accessibility and H3K27ac deposition at *cis*-regulatory elements for both genes (Figure 3G; Figure S4A). Furthermore, GSEA showed significant similarity between the DEGs in *Arid1a*^{cKO} and *Runx3* KO cells (Figure 3I). These data prompted us to compare the numbers and types of WT and *Arid1a*^{cKO} memory CD8$^+$ T cells that form in lymphoid vs. non-lymphoid organs. In the spleen, we observed similar numbers of circulating WT and *Arid1a*^{cKO} TCM and TEM cells (Figure 6B); however, fewer CD127^{lo} terminal TEM (t-TEM) cells were present in the *Arid1a*^{cKO} cells as expected given that this population descends from TE cells[6,48]. Circulating *Arid1a*^{cKO} memory cells were also less proficient in cytokine production after restimulation *ex vivo* (Figure 6C; Figure S6B) and failed to undergo terminal effector differentiation following secondary heterologous infection (Figure 6D), indicating that despite being dispensable for

Author Manuscript Author Manuscript Author Manuscript Author Manuscript

circulating memory cell formation, ARID1A was required for preserving critical memory cell antiviral functions. *Arid1a*^{cKO} memory cells also expressed higher levels of TCF1 (Figure 6E). In contrast to the spleen, in the peripheral tissues such as the liver, small intestine intraepithelial layer (SI-IEL) and salivary gland (SG), there was a profound reduction in the number of Trm cells in the *Arid1a*^{cKO} memory cells relative to the WT controls (Figure 6F; Figure S6C). Further, the memory cells found in the SI-IEL and SG lacking *Arid1a* failed to upregulate several canonical features of Trm, including CD103, CD49a (Figure 6G; Figure S6D), and Granzyme B (Figure 6H), while expression of CD69 and Granzyme A were comparable with WT Trm expression levels (Figure 6G; Figure S6E). *Arid1a*^{cKO} cells infiltrated into the small intestine at slightly lower rates early during infection (Figure S6F), suggesting that the initial seeding of tissues also contributes to, but does not fully account for the diminished Trm pool. Interestingly, as seen in the circulating memory T cells in the spleen (Figure 6E), *Arid1a*^{cKO} Trm maintained high expression of TCF1 (Figure 6I), a known suppressor of Trm formation[49]. This is in spite of the fact that TCF1 was similarly repressed in WT and *Arid1a*^{cKO} early effector cells in both lymphoid tissues and in the SIIEL (Figure S6G). However, cBAF activity was seemingly required to sustain repression of TCF1 as effector cells underwent further effector cell diversification (Figure S6H). Taken together, these results demonstrate that despite observing normal numbers of circulating memory CD8$^+$ T cells, *Arid1a* is required in progenitor cells to open key loci that permit the cells to enter tissues and respond to local cues that induce Trm properties. In summary, we have mapped how cBAF remodels chromatin in virus-specific CD8$^+$ T cells during the first week of infection by creating thousands of enhancers that recruit TFs to cooperatively drive gene expression programs that govern the multitude of effector and memory differentiation states.

Discussion

Effector CD8$^+$ T cell differentiation is a progressive process that occurs over several days to weeks[50], with the earliest known cell fate imprinting events occurring as early as the first cell division[51]. This process is critical to host defense as it generates several types of effector and memory cells that work cooperatively to protect the host from the current infection as well as from future infections. Over the past 15 years the field has discovered many TFs that control the formation of effector and memory CD8$^+$ T cells, but what we don't understand very well is '*how these TFs find their binding sites to regulate target gene expression and T cell differentiation?*' The purpose of this study was to characterize how TF binding sites become accessible within activated CD8$^+$ T cells during an immune response by nucleosome remodeling machinery, like the cBAF complex, to govern the spectrum of effector and memory differentiation states produced.

To address this question, we profiled open chromatin profiles over the first week of infection and found that activated CD8$^+$ T cells simultaneously lose accessibility of naive-associated sites while gaining thousands of activation-induced sites in a time-dependent fashion. Loss of cBAF activity strongly prevented the gain of accessibility at activation-induced sites as early as 48–72 hours post activation *in vivo*, in agreement with a recent report[52]. However, the loss of naive-associated sites upon T cell activation was not affected by cBAF-deficiency. Most ARID1A-dependent OCRs were annotated as enhancers, and

Author Manuscript Author Manuscript Author Manuscript Author Manuscript

indeed many of these sites required ARID1A to become decorated with H3K27ac and enhance transcriptional activation, indicating that cBAF predominantly shapes the enhancer landscape in activated CD8$^+$ T cells. In contrast, several pro-memory genes like *Tcf7*, *Cd9*, *Sell*, and *Ccr7* that become epigenetically silenced via PRC2 (H3K27me3) in late-stage TE cells[53,54] had reduced H3K27me3 and were derepressed in the absence of ARID1A. Notably, cBAF directly antagonizes PRC1, resulting in the redistribution of PRC2 upon deletion/disruption of cBAF subunits, impacting H3K27me3 levels and gene expression both positively and negatively[55–60]. While PRC2 activity is targeted selectively to many pro-memory genes as the effector cells terminally differentiate and lose memory cell potential[35,53,54,61], the mechanism of targeting is unclear. Further dissection of the OCRs and TFs that regulate PRC2 targeting in activated CD8$^+$ T cells will illuminate whether cBAF-dependent remodeling is required for the binding of TFs and associated repressors at these sites, particularly for enhancers bound by TE-inducing TFs, such as T-bet, ZEB2, and Blimp-1[42,62–64], that help to silence such pro-memory loci to enforce terminal differentiation in TE cells.

Our study revealed how cBAF regulates the binding potential of TF families (e.g. ETS, Runt, bZIP, T-box) at enhancers, but not promoters, in activated CD8$^+$ T cells during the first week of infection. Reduced TF binding in *Arid1a*^{cKO} cells can be attributed to a combination of both reduced binding site availability and reduced TF expression. For example, overexpression of T-bet, a factor necessary and sufficient for TE formation, was unable to restore TE differentiation in *Arid1a*-deficient cells that lacked accessible binding sites. Furthermore, pharmacological cBAF disruption in effector cells reduced both chromatin accessibility and T-bet binding within hours, suggesting that cBAF is also required to maintain late-stage TF activity, consistent with recent reports that loss of chromatin accessibility is observed within minutes of acute BAF degradation[65,66]. Given the importance of sustained activity by TFs such as FOXO1 for the active maintenance of long-lived memory cells[67], future work is thus needed to understand the role of continuous cBAF activity in maintaining the longevity and functional competency of effector and memory T cells.

In the absence of ARID1A, activated CD8$^+$ T cells were defective in developing into TE cells, but not circulating TEM or TCM cells. A recent publication from Guo *et al.*[52] similarly found *Arid1a* was important for TE cell formation, but in contrast to our findings, they suggested that disruption of cBAF *enhanced* the formation of memory T cells while we observed no significant difference in memory cells numbers. These differences may be attributed to differences in the timing of *Arid1a* deletion, or incomplete deletion or generation of *Arid1a* heterozygous cells in the CRISPR KO setting. Given that they propose a potential translational application of treating activated CD8$^+$ T cells with BAF inhibitors (BD98) to generate more tenacious anti-tumor T cells for adoptive cell therapy, it is worth emphasizing that our study illuminated that ARID1A-deficient memory precursor cells were epigenetically and transcriptionally aberrant and lacked thousands of enhancers. Moreover, our data indicate that ARID1A-deficient effector and memory cells were less proficient at cytokine production and expressed lower levels of Granzyme A, suggesting potential deficiencies in functionality and cytotoxicity. Therefore, ARID1A is evidently dispensable for some aspects of memory cell differentiation (e.g. clonal expansion of IL-7R$^+$

Author Manuscript Author Manuscript Author Manuscript Author Manuscript

MP-like cells) during LCMV infection, but it is necessary for other key functions and most importantly, for the establishment of tissue residency as elaborated below.

A major finding from our study, which was not explored in Guo *et al.*, is that ARID1A was needed for Trm cell development in non-lymphoid tissues after LCMV infection. Fewer *Arid1a*^{cKO} cells initially infiltrated into the intestines and expressed lower levels of tissue retention molecules, indicating that ARID1A promotes both trafficking into and survival within peripheral tissues. Further, intestinal *Arid1a*^{cKO} cells displayed decreased expression of Trm -signature proteins CD103 and Granzyme B, indicating that these cells were developmentally less mature and likely less protective. Failure of *Arid1a*^{cKO} cells to efficiently form Trm several weeks after infection is likely a consequence of reduced expression of relevant TFs (e.g., *Zfp683*, *Bhlhe40*, *Runx3*) in addition to reduced binding motif accessibility. Runx3 promotes Trm formation in non-lymphoid organs[13], but was downregulated in *Arid1a*^{cKO} MP cells, and the Runt (Runx1/2/3) motif is among those most profoundly lost in KO cells. Likewise, *Bhlhe40* was identified as a core Trm signature gene[13], and was strongly induced in WT effector cells but not in *Arid1a*^{cKO} cells. As was the case with T-bet, overexpression of any individual Trm-associated TF in *Arid1a*^{cKO} cells is unlikely to rescue the Trm formation due to a lack of available binding sites, and because several non-redundant Trm-associated TFs are simultaneously downregulated in these cells. Conversely, *Arid1a*^{cKO} Trm expressed higher levels of TCF1, a factor known to suppress lung Trm formation[49]. In line with these observations, we observed decreased H3K27me3 deposition at the *Tcf7* locus in effector *Arid1a*^{cKO} cells. TGFβ signaling suppresses *Tcf7* expression[49] and drives Trm formation in many tissues[68], and therefore another possible explanation for reduced Trm is that *Arid1a*^{cKO} cells fail to transmit TGFβ signals via SMAD2/3 binding to repress *Tcf7*, a hypothesis supported by the reduction in SMAD3 activity in MP cells as predicted by PageRank analysis. CD8^{+} Trm cells provide protection against mucosal infections[69] and have promising beneficial prognostic value in human tumors[70,71], therefore it will be critical to more carefully examine how BAF inhibitors modulate the differentiation states of TILs in more preclinical models and human T cells as our data demonstrate cBAF is critical for acquisition of Trm differentiation states.

Lastly, this work has high relevance to the understanding of lymphoma etiology because our analysis of *Arid1a*^{cHet} T cells revealed that cBAF operated in a dose-dependent manner to regulate both accessibility and effector cell differentiation states. Most *ARID1A* mutations in human cancers are heterozygous, and in particular, *ARID1A* hemizygosity is common to cutaneous T cell lymphoma[27]. Our data indicate that ARID1A heterozygosity affects accessibility at all sites sensitive to ARID1A loss, resulting in intermediate gene expression changes and cellular phenotypes relative to those of ARID1A-deficient cells. Future work is needed to determine what gene attributes confer sensitivity to ARID1A haploinsufficiency.

In summary, this study characterizes the dynamic regulation of the chromatin landscape in antiviral T cells *in vivo* through the lens of a chromatin remodeler and ascertains how DNA accessibility is created to orchestrate the transcriptional and epigenetic machinery that governs effector and memory CD8^{+} T cell differentiation. We anticipate that ARID1A and cBAF carry out similar biological functions in effector CD4^{+} T cells and other lymphocytes. Indeed, deletion of *Arid1a* or *Smarca4* at various stages of hematopoiesis

Author Manuscript Author Manuscript Author Manuscript Author Manuscript

revealed the critical nature of cBAF in driving development of essentially all hematopoietic lineages[22–24] as well as terminal differentiation of $CD8^+$ T cells[52,72,73] and regulatory T cells[74,75] in tumors. Further, most human pathogenic SNPs map to non-coding regions (i.e. enhancers)[76], implying individual enhancers may have a role in modulating gene expression and influencing cell states. This work thus provides data that may clarify the mechanistic basis for certain human immune-related diseases and establishing new opportunities to fine-tune immune cell function via manipulation of cBAF activity in adoptive cell therapies.

Limitations of the study

Our study primarily relied on the use of Granzyme-B Cre to delete *Arid1a* after T cell activation, and thus we cannot infer what role cBAF may play in early activation (0–48h) events. Secondly, we focused our analysis on memory cells in the spleen and non-lymphoid organs, but it is possible that studying additional lymphoid organs (lymph nodes and bone marrow) may yield further insight into how cBAF more broadly shapes the circulating memory cell pool after infection. Lastly, while we know that cBAF promotes $CD8^+$ T cell expansion, differentiation, and expression of certain cytotoxic molecules (granzyme A) *in vivo*, we have not experimentally assessed whether cBAF is required for cytotoxic capacity.

STAR Methods

RESOURCE AVAILABILITY

Lead Contact—Further information and requests for resources and reagents should be directed to and will be fulfilled by the lead contact, Susan M. Kaech (skaech@salk.edu).

Materials Availability—This study did not generate new unique reagents.

Data and Code Availability—All sequencing data from this paper are available in GEO under accession SuperSeries GSE228381.

EXPERIMENTAL MODEL AND SUBJECT DETAILS

Mice—C57BL/6J were purchased from Jackson Laboratories. P14 mice (Pircher et al., 1987) and $Arid1a^{fl/fl}$mice (Chandler et al., 2015) have been previously described. $Arid1a^{fl/fl}$ GzmB-Cre mice were generated by crossing P14 mice with $Arid1a^{fl/fl}$ and Gzmb-Cre mice. Both female and male mice were used for all studies. Animals were housed in specific-pathogen-free facilities at the Salk Institute. All experimental studies were approved and performed in accordance with guidelines and regulations implemented by the Salk Institute Animal Care and Use Committee.

Infections—Mice were infected with 2×10^5 PFU LCMV-Armstrong by intraperitoneal injection. For recombinant GP33-expressing *Listeria monocytogenes* (LM-GP33) infections, mice were injected with 5×10^4 CFU by retro-orbital injection under anesthesia. LCMV-Armstrong and LM-GP33 stocks were prepared as previously described (Kaech and Ahmed, 2001; Welsh and Seedhom, 2008).

Author Manuscript Author Manuscript Author Manuscript Author Manuscript

Cell Isolation—Spleens, lymph nodes, and livers were mechanically dissociated with 1mL syringe plungers over a 70um nylon strainer. Livers were resuspended in 8mL 40% isotonic percoll and centrifuged at 800g for 12 minutes at 20C. Spleens and livers were incubated in ammonium chloride potassium (ACK) buffer for 5 minutes. For isolation of small intestinal IEL, Peyer's patches were first removed by dissection. Intestines were longitudinally cut and then cut into 1cm pieces and washed in PBS. Pieces were incubated in 30mL HBSS with 10% FBS, 10mM HEPES, and 1mM dithioerythritol with vigorous shaking at 37C for 30 minutes. Supernatants were collected, washed, and further isolated using a 40/67% discontinuous percoll density centrifugation for 20 minutes at room temp with no brakes. Salivary glands were minced with scissors and incubated in RPMI with 5% FBS and 0.5mg/mL Collagenase IV, 0.1mg/mL DNAse1, and 2mM CaCl2 for 30 minutes at 37C with gentle shaking, and then strained over 70um nylon strainers.

Flow Cytometry and cell sorting—Cell suspensions were first incubated with eBioscience Fixable Viability Dye eFluor 780 for 5 minutes at room temp. Cells were stained with primary surface antibodies in PBS with 2% FBS, 0.1% NaN3 for 20 minutes on ice. For sorting, staining was performed in PBS with 2% FBS, 2mM EDTA, and 10mM HEPES. DAPI was added to stained cell suspensions at 0.1ug/mL prior to sorting. For experiments involving retroviral transduction, cells were fixed with Biolegend Fixation buffer for 20 minutes at room temp. For intracellular staining, cells were first fixed with eBioscience Foxp3/Transcription Factor Staining buffer fixation/permeabilization buffer for 30 minutes at room temp, and staining was performed in 1X permeabilization buffer for 30 minutes at room temp. Flow cytometry analysis samples were acquired on a BD Symphony A3. Cell sorting was performed on a BD FACSAria Fusion.

***In vitro* Stimulations and intracellular cytokine staining—**Spleen cell suspensions were stimulated in complete RPMI (RPMI with 10% FBS, Pen/strep, L-glutamine, 50uM β-ME) in the presence of 0.1ng/mL $GP_{33–41}$ peptide or DMSO and brefeldin A for 5 hours at 37C. For cytokine stimulations, cells were cultured for 5 hours with 10ng/mL recombinant mouse IL-12 and IL-18 without brefeldin A, at which point brefeldin A was added for 1 hour prior to staining. Cells were stained for viability and surface markers as described above, and then fixed/permeabilized with cytofix/cytoperm buffer (BD) for 25 minutes at room temp. Intracellular cytokine staining was performed in 1X permeabilization buffer (BD) for 30 minutes at room temp.

Adoptive T cell transfer—Naive WT, $Arid1a^{fl/+}$, or $Arid1a^{fl/fl}$ CD8+ P14 cells were isolated by negative selection with biotinylated antibodies against CD4, CD19, B220, MHCII, CD11b, CD11c, CD49b, and Ter119 in MACS buffer, and MojoSort beads were added at 5% v/v for 5 minutes before placing the cell suspension on a magnet and collecting the supernatant. 2.5×10^4 P14 cells were injected into recipient mice 18–24 hours before infection. For 72h sorting experiments, 5×10^5 P14 cells were transferred. For proliferation experiments, P14 cells were labeled with 5uM CTV (CellTrace Violet) in warm PBS for 8 minutes at 37C, and 1×10^6 cells were transferred. For secondary infection experiments, splenocytes and peripheral LNs from 30d LCMV immune P14 chimeric mice were enriched for $CD127^+$ $CD8^+$ cells. Briefly, negative magnetic selection was performed with

Author Manuscript Author Manuscript Author Manuscript Author Manuscript

biotinylated antibodies against CD4, MHCII, Thy1.2, and KLRG1 in MACS buffer, and MojoSort beads were added at 5% v/v for 5 minutes before placing the cell suspension on a magnet and collecting the supernatant. WT and *Arid1a*^{cKO} memory-enriched populations were mixed to form a 1:1 ratio of WT and *Arid1a*^{cKO} P14 memory cells, and then 6×10^4 memory cells were transferred into naïve recipient mice prior to infection with 1×10^5 CFU of LM-GP33.

Retrovirus production and transduction—Tbet-MIGR1 was previously described (Joshi et al., 2007). Retrovirus was prepared by transfection of 293T cells with pCL-Eco and T-bet-MIGR1 or EV-MIGRs plasmids using XtremeGene9 transfection reagent. For transductions, P14 cells were stimulated for 18 hours with plate-bound 2ug/mL anti-CD3, 1ug/mL anti-CD28, and 20ng/mL human recombinant IL-2. Supernatant was removed from activated cells, and retroviral supernatants supplemented with polybrene (10ug/mL) were carefully overlayed onto cells, and then cells were centrifuged for 90 minutes at 1500g at 30C. Cells were incubated for 4h at 37C, washed, and adoptively transferred into recipient mice.

Cas9 RNP Electroporation—Cas9/sgRNA mixtures were prepared (0.6uL 62nM recombinant Cas9, 0.3nmol sgRNA, 3.5uL RNAse-free H2O) and incubated for 10 minutes at room temperature. $2–5\times10^6$ MACS-purified naive P14 cells were washed in PBS and suspended in 20uL supplemented P3 buffer (Lonza; 16.4uL P3 buffer and 3.6uL Supplement 1). Resuspended cells were immediately mixed with 5uL Cas9/sgRNA mixture and transferred to a Lonza nucleofector strip. Cells were electroporated using the program DN100. 130uL pre-warmed complete RPMI was added to cells prior to incubation for 10 minutes at 37C. Cells were washed extensively with complete RPMI prior to transfer into recipient mice. The sequences of sgRNA used to target *Arid1a*: UACCCAAAUAUGAAUCAAGG.

ATAC-Seq library preparation and sequencing—ATAC-seq was performed as previously described (Corces et al., 2017). Briefly, 5,000–50,000 viable cells were washed with cold PBS, collected by centrifugation, then lysed in resuspension buffer (RSB) (10 mM Tris-HCl, pH 7.4, 10 mM NaCl, 3 mM MgCl2) supplemented with 0.1% NP40, 0.1% Tween-20, and 0.01% digitonin. Samples were incubated on ice for 3 min, then washed out with 1 ml RSB containing 0.1% Tween-20. Nuclei were pelleted by centrifugation at 500g for 10 min at 4°C then resuspended in 50 ul transposition mix (25ul 2x TD buffer, 2.5 ul transposase (100 nM final), 16.5 ul PBS, 0.5 ul 1% digitonin, 0.5 ul 10% Tween-20, 5 ul H_2O) and incubated at 37°C for 30 min in a thermomixer with 1000 RPM mixing. DNA was purified using a Qiagen MinElute PCR cleanup kit, then PCR amplified using indexed oligos. The optimal number of amplification cycles for each sample was determined by qPCR. Libraries were size selected using AmpureXP beads and sequenced using an Illumina NextSeq500 for 75bp paired-end reads.

RNA-Seq library preparation and sequencing—Cells were FACS sorted directly into buffer RLT (Qiagen) supplemented with 2-mercaptoethanol and frozen at −80°C. Total RNA was isolated using a Qiagen RNeasy Plus Micro kit according to the manufacturer's

Author Manuscript Author Manuscript Author Manuscript Author Manuscript

instructions and quantified using an Agilent 4200 TapeStation. Purified RNA was library prepped using a SMART-Seq v4 Ultra Low Input RNA kit. Libraries were quantified and size distribution was determined before 51bp single-end sequencing was performed.

ChIP-seq library preparation and sequencing—Purified polyclonal $CD8^+$ T cells were activated with plate-bound 2ug/mL anti-CD3, 1ug/mL anti-CD28, and 20ng/mL human recombinant IL-2 for 48 hours. Cells were collected and approximately 5×10^6 cells each were treated with either 1μM ACBI1, 300nM BRM04, or 0.01% DMSO for 4 hours. Recombinant mouse IL-12p70 was added after 4 hours culture for an additional 2 hours. Cells were cross linked in 3 mM disuccinimidyl glutarate for 30 min then in 1% formaldehyde for 10 min at room temperature. After quenching with 125 mM glycine, the cells were washed in 1× PBS, pelleted, flash frozen in liquid nitrogen, and stored at 80 °C. Cell pellets were thawed on ice and incubated in lysis solution (50 mM Hepes KOH pH 8, 140 mM NaCl, 1 mM EDTA, 10% glycerol, 0.5% NP-40, and 0.25% Triton X-100) for 10 min. The isolated nuclei were washed (10 mM TrisHCl pH 8, 1 mM EDTA, 0.5 mM EGTA, and 200 mM NaCl) and sheared in (0.1% SDS, 1 mM EDTA, and 10 mM TrisHCl pH 8) with the Covaris E229 sonicator for 10 min. After centrifugation, chromatin was immunoprecipitated overnight at 4 °C with 1:50 T-bet/TBX21 (Cell Signaling Technology, mAb #97135S). The next day, the antibody-bound DNA was incubated with Protein A+G Dynabeads (Invitrogen) in ChIP buffer (50 mM Hepes KOH pH 7.5, 300 mM NaCl, 1 mM EDTA, 1% Triton X-100, 0.1% sodium deoxycholate, and 0.1% SDS), washed, and treated with Proteinase K and RNase A and reverse cross linked. Purified ChIP DNA was used for library generation (NEBNext Ultra II DNA Library Prep Kit for Illumina) according to manufacturer's instructions.

CUT&RUN library preparation and sequencing—CUT&RUN for murine T cells was performed as previously described (Meers et al., 2019) with modifications (van der Veeken et al., 2020). Briefly, 75–150k cells per sample were washed with PBS, counted, and collected in a V-bottom 96 well plate by centrifugation. Cells were washed once in antibody buffer (buffer 1 (1x permeabilization buffer from eBioscience Foxp3/Transcription Factor Staining Buffer Set diluted in nuclease free water, 1X EDTA-free protease inhibitors, 0.5mM spermidine) containing 2mM EDTA), then incubated with antibodies for 1h on ice. After 2 washes in buffer 1, cells were incubated with pA/G-MNase at 1:4000 dilution in buffer 1 for 1h at 4 degrees. Cells were washed twice in buffer 2 (0.05% (w/v) saponin, 1X EDTA-free protease inhibitors, 0.5mM spermidine in PBS) and resuspended in calcium buffer (buffer 2 containing 2mM CaCl2) to activate the MNase fusion protein. Following a 30 minute incubation on wet ice, 2x stop solution (20mM EDTA, 4mM EGTA in buffer 2) was added and cells were incubated for 12 minutes in a 37 degree incubator to release cleaved chromatin fragments. Supernatants were collected by centrifugation and DNA was extracted using a Qiagen MinElute kit.

CUT&RUN libraries were prepared using a NEBNext Ultra II kit. Histone modification sample libraries were prepared according to the manufacturer's protocol, and protein factor samples were prepared according to a factor-specific protocol (Liu, 2021). Briefly, protein factor dA-tailing temperature was decreased to 50°C, and the reaction time was increased

Author Manuscript Author Manuscript Author Manuscript Author Manuscript

to 1 hour. After adaptor ligation, 2.1x volume of AMPure XP beads was added to the reaction to ensure high recovery efficiency of short fragments. After 10–12 cycles of PCR amplification, the reaction was cleaned up with 0.8x AMPureXP beads selection to remove PCR products >350bp, followed by a second round of 1.2X AMPureXP bead size-selection to remove PCR products shorter than 150bp. Barcoded libraries were quantified on an Agilent TapeStation and PCR dimers were removed with 1.2X AmpureXP bead size selection. Samples were mixed at equal molar ratios and pooled libraries were loaded to a NextSeq 300 High Output Kit v2 (150 cycles), and sequenced in the NextSeq 300 platform. To enable determination of fragment length, paired-end sequencing was performed (2×42 bp, 6 bp index).

RNA-seq analysis—Single-end 51-bp reads were aligned to the *M. musculus* mm10 genome using STAR v2.5.3a (Dobin et al., 2013) with default parameters. RNA expression was quantified as raw integer counts using analyzeRepeats.pl in HOMER using the following parameters: -strand both -count exons -condenseGenes -noadj. Differentially expressed genes (DEGs) were identified with getDiffExpression.pl in HOMER using DESeq2 (Love et al., 2014) (cut-offs were set at log2 FC = 0.585 and false discovery rate (FDR) at 0.05 [Benjamini–Hochberg]). GSEA was performed on DEGs against HALLMARK gene sets. For GSEA enrichment plots, fgsea was used with 10,000 permutations = 10,000.

ATAC-Seq analysis—Paired-end 42-bp, or paired-end 75-bp reads were aligned to the *M. musculus* mm10 genome using STAR (Dobin et al., 2013) with default parameters. ATAC-seq peaks were called using the HOMER findPeaks program using parameters for DNAse-seq (-style dnase). Peaks were called when enriched >4.0-fold over local tag counts. Differentially accessible regions were identified using DESeq2 (Love et al., 2014) by calling getDifferentialPeaksReplicates.pl in HOMER with fold change ≥2.0 or ≤−2.0, FDR < 0.05. Peaks sets were annotated with HOMER, and visualizations were created using deepTools. *k*-means clustering of ATAC-seq data was performed using DESeq2. Signal heatmaps were generated using deepTools v3.5.1 (Ramírez et al., 2016).

ChIP-Seq analysis—Paired-end 75-bp reads were aligned to the *M. musculus* mm10 genome using STAR (Dobin et al., 2013) with default parameters. ChIP-seq peaks were called using findPeaks within HOMER using -style factor and an -i input control. Differential ChIP peaks were called using getDiffExpression.pl with fold change ≥ 1.5 or ≤ 1.5, Poisson P value < 0.0001. ChIP-seq peaks were annotated by mapping to the nearest transcription start site (TSS) using the annotatePeaks.pl program. Metaplots were generated using annotatePeaks.pl with parameters -size 2000 and -hist 10. Heatmaps showing overlap of binding sites were generated using mergePeaks in HOMER with flag -matrix, which outputs hypergeometric P values of overlap and the observed/expected ratio of overlap. Peaks sets were annotated with HOMER, and visualizations were created using deepTools.

CUT&RUN analysis—Similar to ChIP-seq analysis, paired-end 75-bp reads were aligned to the *M. musculus* mm10 genome using STAR (Dobin et al., 2013) with default parameters. Peaks were called with Sparse Enrichment Analysis for CUT&RUN (SEACR) with options

Author Manuscript Author Manuscript Author Manuscript Author Manuscript

-stringent and -norm against an IgG control sample (Meers et al., 2019). Metaplots were generated using annotatePeaks.pl with parameters -size 2000 and -hist 10. Heatmaps showing overlap of binding sites were generated using mergePeaks in HOMER with flag -matrix, which outputs hypergeometric P values of overlap and the observed/expected ratio of overlap. Peaks sets were annotated with HOMER, and visualizations were created using deepTools.

Transcription factor binding motif analysis—Sequences within 100 bp of peak centers were compared to known motifs in the HOMER database using the findMotifsGenome.pl (Heinz et al., 2010) command with default parameters. Random GC content-matched genomic regions were used as background. Enriched motifs are statistically significant motifs in input over background by a P value of less than 0.05 using a cumulative binomial distribution.

QUANTIFICATION AND STATISTICAL ANALYSIS

Statistical analyses were performed using the two-tailed, unpaired, Student's t-test unless otherwise specified. Each point represented a biological replicate and all data were presented as the mean ± SEM. The P values were represented as follows: *ns*, not significant, *p<0.05, **p<0.005, ***p<0.0005.

Supplementary Material

Refer to Web version on PubMed Central for supplementary material.

Acknowledgements

We thank the Kaech lab for helpful discussion; N. Claffey, M. Liem at the Salk Flow Cytometry core. This work was supported by NIH grants F31HL158235 and F99CA274688 (B.M.), 5T32GM133351 (B.Y.C), 2T32CA009370 (N.S.A.), R37 AI066232 (to S.M.K.) and AI151123 (to D.C.H.), the Pew-Stewart Scholars for Cancer Research (D.C.H.), and the American Cancer Society Research Scholar Award (D.C.H.) as well as fellowships from the Cancer Research Institute (S.M.), Damon Runyon Cancer Research Foundation (T.M.), and the NOMIS Center (D.C.). Additional support came from the Flow Cytometry Core Facility of the Salk Institute with funding from NIH-NCI CCSG: P30 014195 and Shared Instrumentation Grant S10-OD023689 (Aria Fusion cell sorter) and by the NGS Core Facility of the Salk Institute with funding from NIH-NCI CCSG: P30 014195, the Chapman Foundation and the Helmsley Charitable Trust.

Inclusion and Diversity

One or more of the authors of this paper self-identifies as an underrepresented ethnic minority in their field of research or within their geographical location.

References

1. Kaech SM, and Cui W (2012). Transcriptional control of effector and memory CD8+ T cell differentiation. Nat. Rev. Immunol 12, 749–761. 10.1038/nri3307. [PubMed: 23080391]
2. Gerlach C, Moseman EA, Loughhead SM, Alvarez D, Zwijnenburg AJ, Waanders L, Garg R, de la Torre JC, and von Andrian UH (2016). The Chemokine Receptor CX3CR1 Defines Three Antigen-Experienced CD8 T Cell Subsets with Distinct Roles in Immune Surveillance and Homeostasis. Immunity 45, 1270–1284. 10.1016/j.immuni.2016.10.018. [PubMed: 27939671]

Author Manuscript Author Manuscript Author Manuscript Author Manuscript

3. Kaech SM, Tan JT, Wherry EJ, Konieczny BT, Surh CD, and Ahmed R (2003). Selective expression of the interleukin 7 receptor identifies effector CD8 T cells that give rise to long-lived memory cells. Nat. Immunol 4, 1191–1198. 10.1038/ni1009. [PubMed: 14625547]

4. Cui W, Joshi NS, Jiang A, and Kaech SM (2009). Effects of Signal 3 during CD8 T cell priming: Bystander production of IL-12 enhances effector T cell expansion but promotes terminal differentiation. Vaccine 27, 2177–2187. 10.1016/j.vaccine.2009.01.088. [PubMed: 19201385]

5. Herndler-Brandstetter D, Ishigame H, Shinnakasu R, Plajer V, Stecher C, Zhao J, Lietzenmayer M, Kroehling L, Takumi A, Kometani K, et al. (2018). KLRG1+ Effector CD8+ T Cells Lose KLRG1, Differentiate into All Memory T Cell Lineages, and Convey Enhanced Protective Immunity. Immunity 48, 716–729.e8. 10.1016/j.immuni.2018.03.015. [PubMed: 29625895]

6. Joshi NS, Cui W, Chandele A, Lee HK, Urso DR, Hagman J, Gapin L, and Kaech SM (2007). Inflammation directs memory precursor and short-lived effector CD8(+) T cell fates via the graded expression of T-bet transcription factor. Immunity 27, 281–295. 10.1016/j.immuni.2007.07.010. [PubMed: 17723218]

7. Obar JJ, Jellison ER, Sheridan BS, Blair DA, Pham Q-M, Zickovich JM, and Lefrançois L (2011). Pathogen-Induced Inflammatory Environment Controls Effector and Memory CD8+ T Cell Differentiation. J. Immunol 187, 4967–4978. 10.4049/jimmunol.1102335. [PubMed: 21987662]

8. Plumlee CR, Obar JJ, Colpitts SL, Jellison ER, Haining WN, Lefrancois L, and Khanna KM (2015). Early Effector CD8 T Cells Display Plasticity in Populating the Short-Lived Effector and Memory-Precursor Pools Following Bacterial or Viral Infection. Sci. Rep 5, 12264. 10.1038/srep12264. [PubMed: 26191658]

9. Behr FM, Parga-Vidal L, Kragten NAM, van Dam TJP, Wesselink TH, Sheridan BS, Arens R, van Lier RAW, Stark R, and van Gisbergen KPJM (2020). Tissue-resident memory CD8+ T cells shape local and systemic secondary T cell responses. Nat. Immunol 21, 1070–1081. 10.1038/s41590-020-0723-4. [PubMed: 32661361]

10. Mackay LK, Minnich M, Kragten NAM, Liao Y, Nota B, Seillet C, Zaid A, Man K, Preston S, Freestone D, et al. (2016). Hobit and Blimp1 instruct a universal transcriptional program of tissue residency in lymphocytes. Science 352, 459–463. 10.1126/science.aad2035. [PubMed: 27102484]

11. Gautam S, Fioravanti J, Zhu W, Le Gall JB, Brohawn P, Lacey NE, Hu J, Hocker JD, Hawk NV, Kapoor V, et al. (2019). The transcription factor c-Myb regulates CD8+ T cell stemness and antitumor immunity. Nat. Immunol 20, 337–349. 10.1038/s41590-018-0311-z. [PubMed: 30778251]

12. Li C, Zhu B, Son YM, Wang Z, Jiang L, Xiang M, Ye Z, Beckermann KE, Wu Y, Jenkins JW, et al. (2019). The Transcription Factor Bhlhe40 Programs Mitochondrial Regulation of Resident CD8+ T Cell Fitness and Functionality. Immunity 51, 491–507.e7. 10.1016/j.immuni.2019.08.013. [PubMed: 31533057]

13. Milner JJ, Toma C, Yu B, Zhang K, Omilusik K, Phan AT, Wang D, Getzler AJ, Nguyen T, Crotty S, et al. (2017). Runx3 programs CD8+ T cell residency in non-lymphoid tissues and tumours. Nature 552, 253–257. 10.1038/nature24993. [PubMed: 29211713]

14. Doering TA, Crawford A, Angelosanto JM, Paley MA, Ziegler CG, and Wherry EJ (2012). Network analysis reveals centrally connected genes and pathways involved in CD8+ T cell exhaustion versus memory. Immunity 37, 1130–1144. 10.1016/j.immuni.2012.08.021. [PubMed: 23159438]

15. Hargreaves DC, and Crabtree GR (2011). ATP-dependent chromatin remodeling: genetics, genomics and mechanisms. Cell Res 21, 396–420. 10.1038/cr.2011.32. [PubMed: 21358755]

16. Alpsoy A, and Dykhuizen EC (2018). Glioma tumor suppressor candidate region gene 1 (GLTSCR1) and its paralog GLTSCR1-like form SWI/SNF chromatin remodeling subcomplexes. J. Biol. Chem 293, 3892–3903. 10.1074/jbc.RA117.001065. [PubMed: 29374058]

17. Gatchalian J, Malik S, Ho J, Lee D-S, Kelso TWR, Shokhirev MN, Dixon JR, and Hargreaves DC (2018). A non-canonical BRD9-containing BAF chromatin remodeling complex regulates naive pluripotency in mouse embryonic stem cells. Nat. Commun 9, 5139. 10.1038/s41467-018-07528-9. [PubMed: 30510198]

18. Mashtalir N, D'Avino AR, Michel BC, Luo J, Pan J, Otto JE, Zullow HJ, McKenzie ZM, Kubiak RL, St Pierre R, et al. (2018). Modular Organization and Assembly of SWI/SNF

Author Manuscript Author Manuscript Author Manuscript Author Manuscript

Family Chromatin Remodeling Complexes. Cell 175, 1272–1288.e20. 10.1016/j.cell.2018.09.032. [PubMed: 30343899]

19. Blümli S, Wiechens N, Wu M-Y, Singh V, Gierlinski M, Schweikert G, Gilbert N, Naughton C, Sundaramoorthy R, Varghese J, et al. (2021). Acute depletion of the ARID1A subunit of SWI/SNF complexes reveals distinct pathways for activation and repression of transcription. Cell Rep. 37, 109943. 10.1016/j.celrep.2021.109943. [PubMed: 34731603]
20. Kelso TWR, Porter DK, Amaral ML, Shokhirev MN, Benner C, and Hargreaves DC (2017). Chromatin accessibility underlies synthetic lethality of SWI/SNF subunits in ARID1A-mutant cancers. eLife 6, e30506. 10.7554/eLife.30506. [PubMed: 28967863]
21. Mathur R, Alver BH, San Roman AK, Wilson BG, Wang X, Agoston AT, Park PJ, Shivdasani RA, and Roberts CWM (2017). ARID1A loss impairs enhancer-mediated gene regulation and drives colon cancer in mice. Nat. Genet 49, 296–302. 10.1038/ng.3744. [PubMed: 27941798]
22. Astori A, Tingvall-Gustafsson J, Kuruvilla J, Coyaud E, Laurent EMN, Sunnerhagen M, Åhsberg J, Ungerbäck J, Strid T, Sigvardsson M, et al. (2020). ARID1a Associates with Lymphoid-Restricted Transcription Factors and Has an Essential Role in T Cell Development. J. Immunol. Baltim. Md 1950 205, 1419–1432. 10.4049/jimmunol.1900959.
23. Chi TH, Wan M, Lee PP, Akashi K, Metzger D, Chambon P, Wilson CB, and Crabtree GR (2003). Sequential roles of Brg, the ATPase subunit of BAF chromatin remodeling complexes, in thymocyte development. Immunity 19, 169–182. 10.1016/s1074-7613(03)00199-7. [PubMed: 12932351]
24. Han L, Madan V, Mayakonda A, Dakle P, Woon TW, Shyamsunder P, Nordin HBM, Cao Z, Sundaresan J, Lei I, et al. (2019). Chromatin remodeling mediated by ARID1A is indispensable for normal hematopoiesis in mice. Leukemia 33, 2291–2305. 10.1038/s41375-019-0438-4. [PubMed: 30858552]
25. Kadoch C, and Crabtree GR (2015). Mammalian SWI/SNF chromatin remodeling complexes and cancer: Mechanistic insights gained from human genomics. Sci. Adv 1, e1500447. 10.1126/sciadv.1500447. [PubMed: 26601204]
26. Kadoch C, Hargreaves DC, Hodges C, Elias L, Ho L, Ranish J, and Crabtree GR (2013). Proteomic and bioinformatic analysis of mammalian SWI/SNF complexes identifies extensive roles in human malignancy. Nat. Genet 45, 592–601. 10.1038/ng.2628. [PubMed: 23644491]
27. Choi J, Goh G, Walradt T, Hong BS, Bunick CG, Chen K, Bjornson RD, Maman Y, Wang T, Tordoff J, et al. (2015). Genomic landscape of cutaneous T cell lymphoma. Nat. Genet 47, 1011–1019. 10.1038/ng.3356. [PubMed: 26192916]
28. Wang L, Ni X, Covington KR, Yang BY, Shiu J, Zhang X, Xi L, Meng Q, Langridge T, Drummond J, et al. (2015). Genomic profiling of Sézary Syndrome identifies alterations of key T-cell signaling and differentiation genes. Nat. Genet 47, 1426–1434. 10.1038/ng.3444. [PubMed: 26551670]
29. Scharer CD, Bally APR, Gandham B, and Boss JM (2017). Cutting Edge: Chromatin Accessibility Programs CD8 T Cell Memory. J. Immunol 198, 2238–2243. 10.4049/jimmunol.1602086. [PubMed: 28179496]
30. Scott-Browne JP, López-Moyado IF, Trifari S, Wong V, Chavez L, Rao A, and Pereira RM (2016). Dynamic Changes in Chromatin Accessibility Occur in CD8+ T Cells Responding to Viral Infection. Immunity 45, 1327–1340. 10.1016/j.immuni.2016.10.028. [PubMed: 27939672]
31. Pircher H, Michalopoulos EE, Iwamoto A, Ohashi PS, Baenziger J, Hengartner H, Zinkernagel RM, and Mak TW (1987). Molecular analysis of the antigen receptor of virus-specific cytotoxic T cells and identification of a new V alpha family. Eur. J. Immunol 17, 1843–1846. 10.1002/eji.1830171226. [PubMed: 2961577]
32. Buenrostro JD, Giresi PG, Zaba LC, Chang HY, and Greenleaf WJ (2013). Transposition of native chromatin for fast and sensitive epigenomic profiling of open chromatin, DNA-binding proteins and nucleosome position. Nat. Methods 10, 1213–1218. 10.1038/nmeth.2688. [PubMed: 24097267]
33. Skene PJ, and Henikoff S (2017). An efficient targeted nuclease strategy for high-resolution mapping of DNA binding sites. eLife 6, e21856. 10.7554/eLife.21856. [PubMed: 28079019]
34. Corces MR, Buenrostro JD, Wu B, Greenside PG, Chan SM, Koenig JL, Snyder MP, Pritchard JK, Kundaje A, Greenleaf WJ, et al. (2016). Lineage-specific and single-cell chromatin accessibility

Author Manuscript Author Manuscript Author Manuscript Author Manuscript

charts human hematopoiesis and leukemia evolution. Nat. Genet 48, 1193–1203. 10.1038/ng.3646. [PubMed: 27526324]

35. Yu B, Zhang K, Milner JJ, Toma C, Chen R, Scott-Browne JP, Pereira RM, Crotty S, Chang JT, Pipkin ME, et al. (2017). Epigenetic landscapes reveal transcription factors that regulate CD8+ T cell differentiation. Nat. Immunol 18, 573–582. 10.1038/ni.3706. [PubMed: 28288100]
36. Kurachi M, Barnitz RA, Yosef N, Odorizzi PM, DiIorio MA, Lemieux ME, Yates K, Godec J, Klatt MG, Regev A, et al. (2014). The transcription factor BATF operates as an essential differentiation checkpoint in early effector CD8+ T cells. Nat. Immunol 15, 373–383. 10.1038/ni.2834. [PubMed: 24584090]
37. Tsao H-W, Kaminski J, Kurachi M, Barnitz RA, DiIorio MA, LaFleur MW, Ise W, Kurosaki T, Wherry EJ, Haining WN, et al. (2022). Batf-mediated epigenetic control of effector CD8+ T cell differentiation. Sci. Immunol 7, eabi4919. 10.1126/sciimmunol.abi4919.
38. Zhong Y, Walker SK, Pritykin Y, Leslie CS, Rudensky AY, and van der Veeken J (2022). Hierarchical regulation of the resting and activated T cell epigenome by major transcription factor families. Nat. Immunol 23, 122–134. 10.1038/s41590-021-01086-x. [PubMed: 34937932]
39. Jacob J, and Baltimore D (1999). Modelling T-cell memory by genetic marking of memory T cells in vivo. Nature 399, 593–597. 10.1038/21208. [PubMed: 10376601]
40. Subramanian A, Tamayo P, Mootha VK, Mukherjee S, Ebert BL, Gillette MA, Paulovich A, Pomeroy SL, Golub TR, Lander ES, et al. (2005). Gene set enrichment analysis: a knowledge-based approach for interpreting genome-wide expression profiles. Proc. Natl. Acad. Sci. U. S. A 102, 15545–15550. 10.1073/pnas.0506580102. [PubMed: 16199517]
41. Marchingo JM, Sinclair LV, Howden AJ, and Cantrell DA (2020). Quantitative analysis of how Myc controls T cell proteomes and metabolic pathways during T cell activation. eLife 9, e53725. 10.7554/eLife.53725.
42. Dominguez CX, Amezquita RA, Guan T, Marshall HD, Joshi NS, Kleinstein SH, and Kaech SM (2015). The transcription factors ZEB2 and T-bet cooperate to program cytotoxic T cell terminal differentiation in response to LCMV viral infection. J. Exp. Med 212, 2041–2056. 10.1084/jem.20150186. [PubMed: 26503446]
43. Prier JE, Li J, Gearing LJ, Olshansky M, Sng XYX, Hertzog PJ, and Turner SJ (2019). Early T-BET Expression Ensures an Appropriate CD8+ Lineage-Specific Transcriptional Landscape after Influenza A Virus Infection. J. Immunol. Baltim. Md 1950 203, 1044–1054. 10.4049/jimmunol.1801431.
44. Shan Q, Zeng Z, Xing S, Li F, Hartwig SM, Gullicksrud JA, Kurup SP, Van Braeckel-Budimir N, Su Y, Martin MD, et al. (2017). The transcription factor Runx3 guards cytotoxic CD8+ effector T cells against deviation towards follicular helper T cell lineage. Nat. Immunol 18, 931–939. 10.1038/ni.3773. [PubMed: 28604718]
45. Farnaby W, Koegl M, Roy MJ, Whitworth C, Diers E, Trainor N, Zollman D, Steurer S, Karolyi-Oezguer J, Riedmueller C, et al. (2019). BAF complex vulnerabilities in cancer demonstrated via structure-based PROTAC design. Nat. Chem. Biol 15, 672–680. 10.1038/s41589-019-0294-6. [PubMed: 31178587]
46. Papillon JPN, Nakajima K, Adair CD, Hempel J, Jouk AO, Karki RG, Mathieu S, Möbitz H, Ntaganda R, Smith T, et al. (2018). Discovery of Orally Active Inhibitors of Brahma Homolog (BRM)/SMARCA2 ATPase Activity for the Treatment of Brahma Related Gene 1 (BRG1)/SMARCA4-Mutant Cancers. J. Med. Chem 61, 10155–10172. 10.1021/acs.jmedchem.8b01318. [PubMed: 30339381]
47. Zhang K, Wang M, Zhao Y, and Wang W (2019). Taiji: System-level identification of key transcription factors reveals transcriptional waves in mouse embryonic development. Sci. Adv 5, eaav3262. 10.1126/sciadv.aav3262.
48. Milner JJ, Nguyen H, Omilusik K, Reina-Campos M, Tsai M, Toma C, Delpoux A, Boland BS, Hedrick SM, Chang JT, et al. (2020). Delineation of a molecularly distinct terminally differentiated memory CD8 T cell population. Proc. Natl. Acad. Sci. U. S. A 117, 25667–25678. 10.1073/pnas.2008571117. [PubMed: 32978300]
49. Wu J, Madi A, Mieg A, Hotz-Wagenblatt A, Weisshaar N, Ma S, Mohr K, Schlimbach T, Hering M, Borgers H, et al. (2020). T Cell Factor 1 Suppresses CD103+ Lung Tissue-Resident Memory T Cell Development. Cell Rep. 31, 107484. 10.1016/j.celrep.2020.03.048. [PubMed: 32268106]

Author Manuscript Author Manuscript Author Manuscript Author Manuscript

50. Youngblood B, Hale JS, Kissick HT, Ahn E, Xu X, Wieland A, Araki K, West EE, Ghoneim HE, Fan Y, et al. (2017). EFFECTOR CD8 T CELLS DEDIFFERENTIATE INTO LONG-LIVED MEMORY CELLS. Nature 552, 404–409. 10.1038/nature25144. [PubMed: 29236683]
51. Chang JT, Ciocca ML, Kinjyo I, Palanivel VR, McClurkin CE, DeJong CS, Mooney EC, Kim JS, Steinel NC, Oliaro J, et al. (2011). Asymmetric Proteasome Segregation as a Mechanism for Unequal Partitioning of the Transcription Factor T-bet during T Lymphocyte Division. Immunity 34, 492–504. 10.1016/j.immuni.2011.03.017. [PubMed: 21497118]
52. Guo A, Huang H, Zhu Z, Chen MJ, Shi H, Yuan S, Sharma P, Connelly JP, Liedmann S, Dhungana Y, et al. (2022). cBAF complex components and MYC cooperate early in CD8+ T cell fate. Nature. 10.1038/s41586-022-04849-0.
53. Gray SM, Amezquita RA, Guan T, Kleinstein SH, and Kaech SM (2017). Polycomb Repressive Complex 2-Mediated Chromatin Repression Guides Effector CD8+ T Cell Terminal Differentiation and Loss of Multipotency. Immunity 46, 596–608. 10.1016/j.immuni.2017.03.012. [PubMed: 28410989]
54. Kakaradov B, Arsenio J, Widjaja CE, He Z, Aigner S, Metz PJ, Yu B, Wehrens EJ, Lopez J, Kim SH, et al. (2017). Early transcriptional and epigenetic regulation of CD8+ T cell differentiation revealed by single-cell RNA-seq. Nat. Immunol 18, 422–432. 10.1038/ni.3688. [PubMed: 28218746]
55. Braun SMG, Kirkland JG, Chory EJ, Husmann D, Calarco JP, and Crabtree GR (2017). Rapid and reversible epigenome editing by endogenous chromatin regulators. Nat. Commun 8, 560. 10.1038/s41467-017-00644-y. [PubMed: 28916764]
56. Ho L, Miller EL, Ronan JL, Ho W, Jothi R, and Crabtree GR (2011). esBAF Facilitates Pluripotency by Conditioning the Genome for LIF/STAT3Signalingand by Regulating Polycomb Function. Nat. Cell Biol 13, 903–913. 10.1038/ncb2285. [PubMed: 21785422]
57. Kadoch C, Williams RT, Calarco JP, Miller EL, Weber CM, Braun SMG, Pulice JL, Chory EJ, and Crabtree GR (2017). Dynamics of BAF-Polycomb complex opposition on heterochromatin in normal and oncogenic states. Nat. Genet 49, 213–222. 10.1038/ng.3734. [PubMed: 27941796]
58. Nakayama RT, Pulice JL, Valencia AM, McBride MJ, McKenzie ZM, Gillespie MA, Ku WL, Teng M, Cui K, Williams RT, et al. (2017). SMARCB1 is required for widespread BAF complex-mediated activation of enhancers and bivalent promoters. Nat. Genet 49, 1613–1623. 10.1038/ng.3958. [PubMed: 28945250]
59. Stanton BZ, Hodges C, Calarco JP, Braun SMG, Ku WL, Kadoch C, Zhao K, and Crabtree GR (2017). Smarca4 ATPase mutations disrupt direct eviction of PRC1 from chromatin. Nat. Genet 49, 282–288. 10.1038/ng.3735. [PubMed: 27941795]
60. Weber CM, Hafner A, Kirkland JG, Braun SMG, Stanton BZ, Boettiger AN, and Crabtree GR (2021). mSWI/SNF promotes Polycomb repression both directly and through genome-wide redistribution. Nat. Struct. Mol. Biol 28, 501–511. 10.1038/s41594-021-00604-7. [PubMed: 34117481]
61. Pace L, Goudot C, Zueva E, Gueguen P, Burgdorf N, Waterfall JJ, Quivy J-P, Almouzni G, and Amigorena S (2018). The epigenetic control of stemness in CD8+ T cell fate commitment. Science 359, 177–186. 10.1126/science.aah6499. [PubMed: 29326266]
62. Oestreich KJ, and Weinmann AS (2012). T-bet employs diverse regulatory mechanisms to repress transcription. Trends Immunol. 33, 78–83. 10.1016/j.it.2011.10.005. [PubMed: 22133865]
63. Omilusik KD, Best JA, Yu B, Goossens S, Weidemann A, Nguyen JV, Seuntjens E, Stryjewska A, Zweier C, Roychoudhuri R, et al. (2015). Transcriptional repressor ZEB2 promotes terminal differentiation of CD8+ effector and memory T cell populations during infection. J. Exp. Med 212, 2027–2039. 10.1084/jem.20150194. [PubMed: 26503445]
64. Rutishauser RL, Martins GA, Kalachikov S, Chandele A, Parish IA, Meffre E, Jacob J, Calame K, and Kaech SM (2009). Transcriptional repressor Blimp-1 promotes CD8(+) T cell terminal differentiation and represses the acquisition of central memory T cell properties. Immunity 31, 296–308. 10.1016/j.immuni.2009.05.014. [PubMed: 19664941]
65. Iurlaro M, Stadler MB, Masoni F, Jagani Z, Galli GG, and Schübeler D (2021). Mammalian SWI/SNF continuously restores local accessibility to chromatin. Nat. Genet 53, 279–287. 10.1038/s41588-020-00768-w. [PubMed: 33558757]

Author Manuscript Author Manuscript Author Manuscript Author Manuscript

66. Schick S, Grosche S, Kohl KE, Drpic D, Jaeger MG, Marella NC, Imrichova H, Lin J-MG, Hofstätter G, Schuster M, et al. (2021). Acute BAF perturbation causes immediate changes in chromatin accessibility. Nat. Genet 53, 269–278. 10.1038/s41588-021-00777-3. [PubMed: 33558760]

67. Delpoux A, Michelini RH, Verma S, Lai C-Y, Omilusik KD, Utzschneider DT, Redwood AJ, Goldrath AW, Benedict CA, and Hedrick SM (2018). Continuous activity of Foxo1 is required to prevent anergy and maintain the memory state of CD8+ T cells. J. Exp. Med 215, 575–594. 10.1084/jem.20170697. [PubMed: 29282254]

68. Zhang N, and Bevan MJ (2013). Transforming growth factor-β signaling controls the formation and maintenance of gut-resident memory T cells by regulating migration and retention. Immunity 39, 687–696. 10.1016/j.immuni.2013.08.019. [PubMed: 24076049]

69. Schenkel JM, and Masopust D (2014). Tissue-Resident Memory T Cells. Immunity 41, 886–897. 10.1016/j.immuni.2014.12.007. [PubMed: 25526304]

70. Amsen D, van Gisbergen KPJM, Hombrink P, and van Lier RAW (2018). Tissue-resident memory T cells at the center of immunity to solid tumors. Nat. Immunol 19, 538–546. 10.1038/s41590-018-0114-2. [PubMed: 29777219]

71. Okła K, Farber DL, and Zou W (2021). Tissue-resident memory T cells in tumor immunity and immunotherapy. J. Exp. Med 218, e20201605. 10.1084/jem.20201605.

72. Belk JA, Yao W, Ly N, Freitas KA, Chen Y-T, Shi Q, Valencia AM, Shifrut E, Kale N, Yost KE, et al. (2022). Genome-wide CRISPR screens of T cell exhaustion identify chromatin remodeling factors that limit T cell persistence. Cancer Cell, S1535610822002318. 10.1016/j.ccell.2022.06.001.

73. Battistello E, Hixon KA, Comstock DE, Collings CK, Chen X, Rodriguez Hernaez J, Lee S, Cervantes KS, Hinkley MM, Ntatsoulis K, et al. (2023). Stepwise activities of mSWI/SNF family chromatin remodeling complexes direct T cell activation and exhaustion. Mol. Cell 10.1016/j.molcel.2023.02.026.

74. Long L, Wei J, Lim SA, Raynor JL, Shi H, Connelly JP, Wang H, Guy C, Xie B, Chapman NM, et al. (2021). CRISPR screens unveil signal hubs for nutrient licensing of T cell immunity. Nature 600, 308–313. 10.1038/s41586-021-04109-7. [PubMed: 34795452]

75. Loo C-S, Gatchalian J, Liang Y, Leblanc M, Xie M, Ho J, Venkatraghavan B, Hargreaves DC, and Zheng Y (2020). A Genome-wide CRISPR Screen Reveals a Role for the Non-canonical Nucleosome-Remodeling BAF Complex in Foxp3 Expression and Regulatory T Cell Function. Immunity 53, 143–157.e8. 10.1016/j.immuni.2020.06.011. [PubMed: 32640256]

76. Corradin O, and Scacheri PC (2014). Enhancer variants: evaluating functions in common disease. Genome Med. 6, 85. 10.1186/s13073-014-0085-3. [PubMed: 25473424]

Author Manuscript Author Manuscript Author Manuscript Author Manuscript

Highlights

- ARID1A-containing cBAF opens enhancers in effector $CD8^+$ T cells during infection
- cBAF establishes binding sites of many effector TFs, including T-bet and BATF
- cBAF is necessary for late-stage differentiation of TE and Trm cells
- Circulating memory cells form without cBAF, but are functionally impaired

Author Manuscript
Author Manuscript
Author Manuscript
Author Manuscript

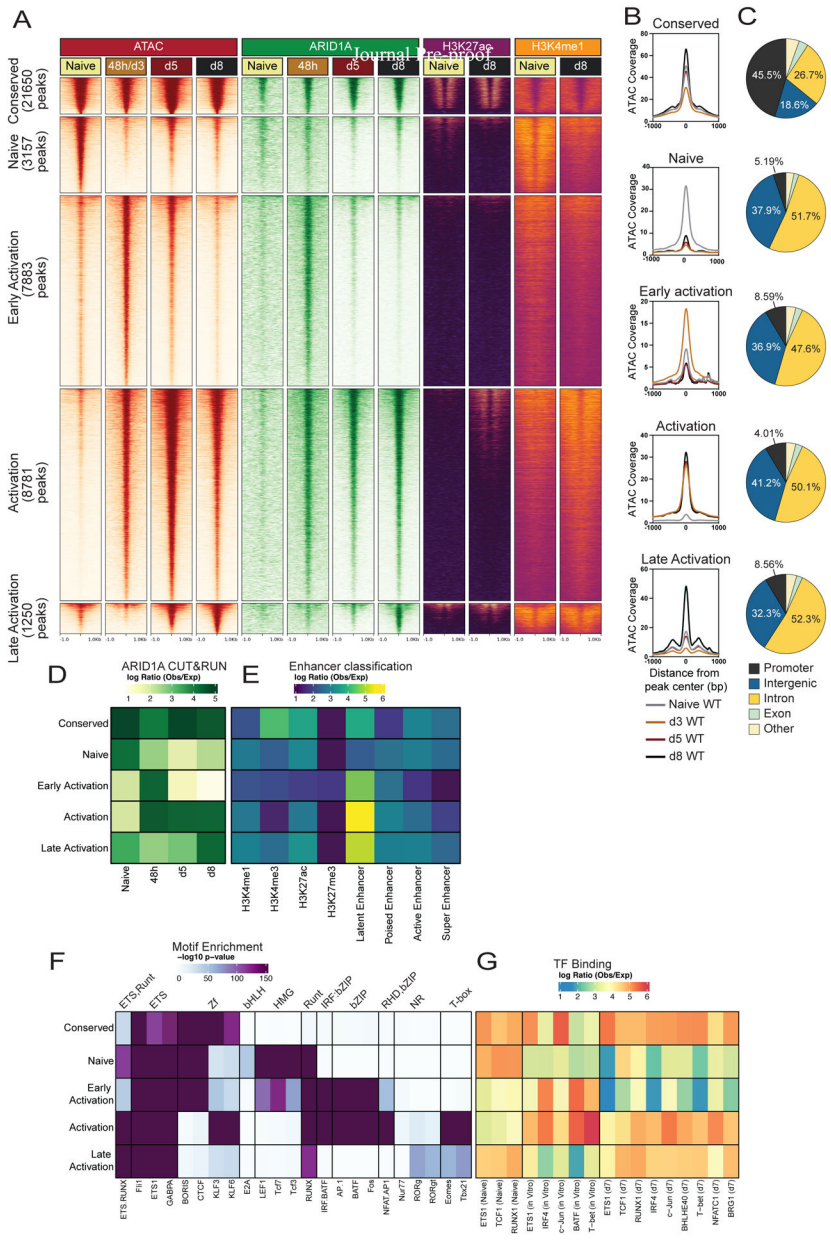

Fig. 1. Differentiating antiviral effector CD8$^+$ T cells exhibit highly dynamic accessible chromatin and cBAF occupancy patterns.

(A) Signal tracks of ATAC-seq, ARID1A C&R, H3K27ac ChIP-Seq and H3K4me1 ChIP-Seq (GSE89036) in naïve, 48h *in vitro* activated, or d3, d5, or d8 P14 CD8$^+$ T cells from LCMV-Armstrong infection. (B) ATAC-seq signal coverage and (C) annotation of OCRs from clusters in A. (D-G) Using the OCRs from clusters in (A) we correlated those with ARID1A binding (D), histone modifications to define enhancers (E), predicted TF motif enrichment (F) and actual TF binding (observed/expected) of the indicated TFs from public datasets (GSE54191, GSE192390, GSE166718) (G).

Author Manuscript Author Manuscript Author Manuscript Author Manuscript

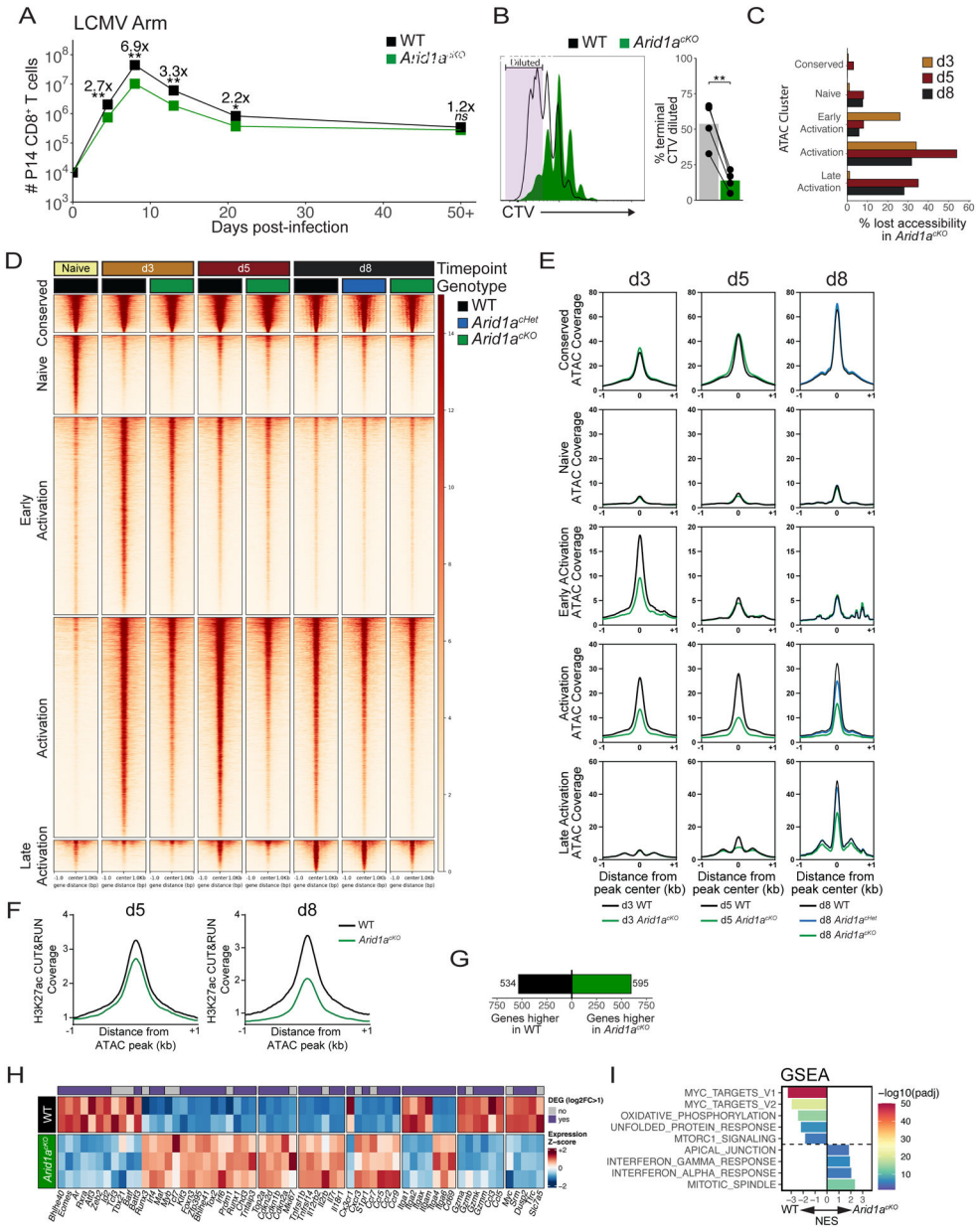

Fig 2. Arid1a promotes clonal expansion and opening of activation-induced enhancers.

(A) Numbers of WT (black) and *Arid1a*^{cKO} (green) P14 cells after infection with LCMV-Armstrong. n=8 (d4.5), 8–11 (d8), 4 (d13), 4 (d21), 8 (d50+). (B) CellTrace Violet dilution of WT and *Arid1a*^{cKO} P14 cells at 84h p.i. Frequency of cells that divided 7+ times are quantified in the bar graph. (C) Percentage of ATAC-seq peaks lost (2-fold change, FDR<0.05, Benjamini-Hochberg) in *Arid1a*^{cKO} relative to WT cells at d3, d5, and d8 p.i. (D, E) ATAC-seq signal coverage of WT and *Arid1a*^{cKO} P14 cells at d3, d5, and d8 p.i. using the same cluster designations defined in Figure 1A. (F) H3K27ac CUT&RUN signal coverage centered on ATAC-seq peaks in WT vs. *Arid1a*^{cKO} cells. (G-I) WT and *Arid1a*^{cKO} effector cells were isolated at d3 p.i. and compared for differentially expressed genes (DEGs) by RNA-sequencing (>2-fold change, adjusted p-value<0.05, Benjamini-Hochberg). Number of

Author Manuscript Author Manuscript Author Manuscript Author Manuscript

DEGs (G), heatmap of biologically relevant DEGs (H), and gene set enrichment analysis (GSEA) (I) between WT and *Arid1a*^{cKO} effector cells are shown. All heatmap genes shown have an adjusted p-value < 0.05. (I) Top 8 Hallmark gene sets (adjusted p value < 0.01, 10,000 permutations) are shown. *ns*, not significant; *p<0.05, **p<0.005.

Author Manuscript Author Manuscript Author Manuscript Author Manuscript

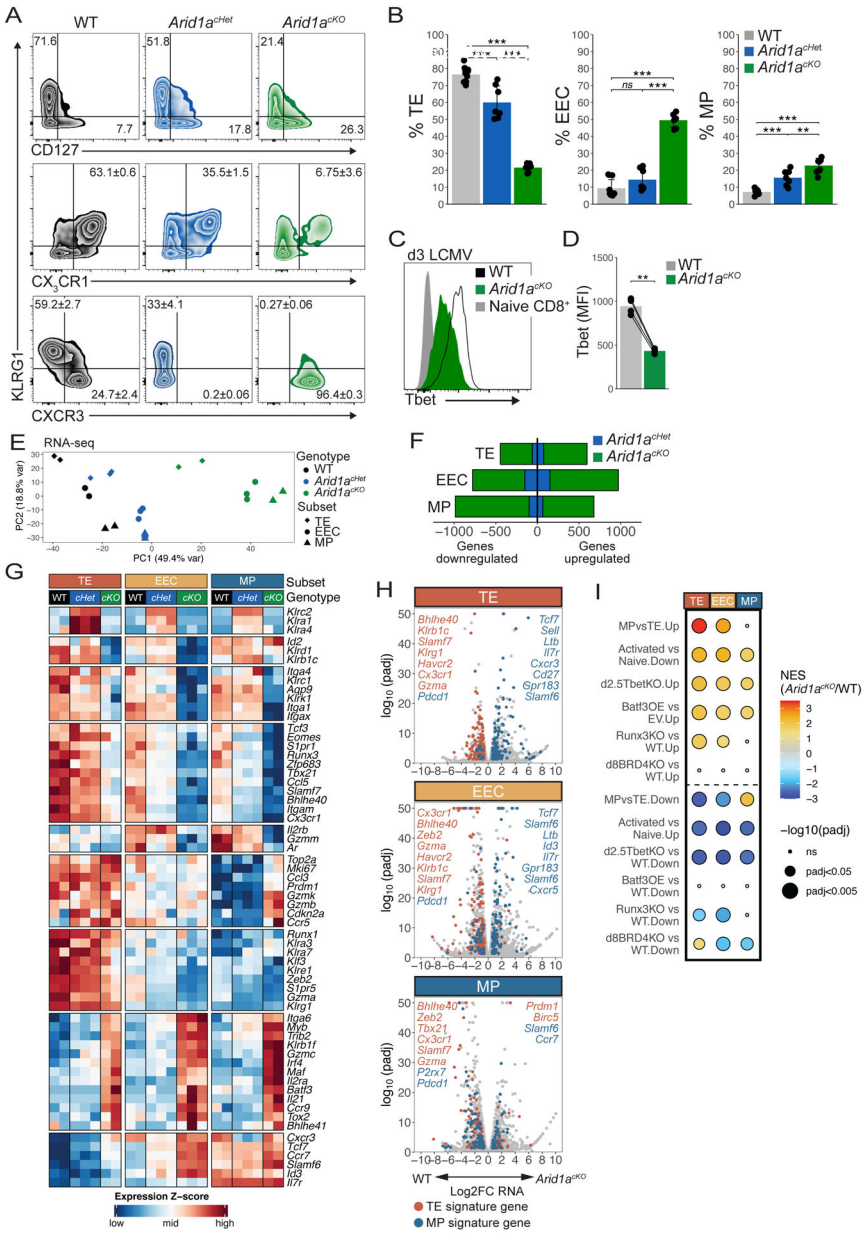

Fig 3. *Arid1a* acts in a dose-dependent manner to specify effector subset gene expression patterns

(A,B) Surface marker expression of WT (black, n=11), *Arid1a*^{cHet} (blue, n=7), and *Arid1a*^{cKO} (green, n=7) P14 cells at d8–9 p.i. was analyzed by flow cytometry (A) and mean ± SEM frequencies of TE (KLRG1^{+}CD127^{-}), MP (KLRG1^{-}CD127^{+}), KLRG1^{+}CX$_3$CR1^{+}, KLRG1^{+}CXCR3^{-}, and KLRG1^{-}CXCR3^{+} cells are shown in bar graphs (B). (C,D) T-bet expression in WT and *Arid1a*^{cKO} P14 cells at d3 p.i. (D) Paired t-test. (E-I) WT, *Arid1a*^{cKO} and *Arid1a*^{cHet} effector cells were isolated at d8 p.i. and sorted based on expression of TE, EEC and MP markers as defined in (A) and differentially expressed genes (DEGs) were identified by RNA-seq. Principal component analysis plot of all the samples (E), number of DEGs (F), heatmap of select DEGs (G), volcano plots of all DEGs including highlighted TE-signature genes (red) and MP-signature genes (blue) (H), and GSEA (I) were used to

Author Manuscript Author Manuscript Author Manuscript Author Manuscript

assess the DEGs in each subset affected by loss of one or two copies of *Arid1a*. GSEA analysis in (I) directly compared DEGs between WT and *Arid1a*^{cKO} cells and previously published datasets: Activated vs Naive: GSE10739; d2.5TbetKO: PRJNA547650; Batf3OE vs EV: GSE143504; Runx3KO: GSE81888; d8BRD4KO: GSE173515). *ns*, not significant; *p<0.05, **p<0.005, ***p<0.0005.

Author Manuscript
Author Manuscript
Author Manuscript
Author Manuscript

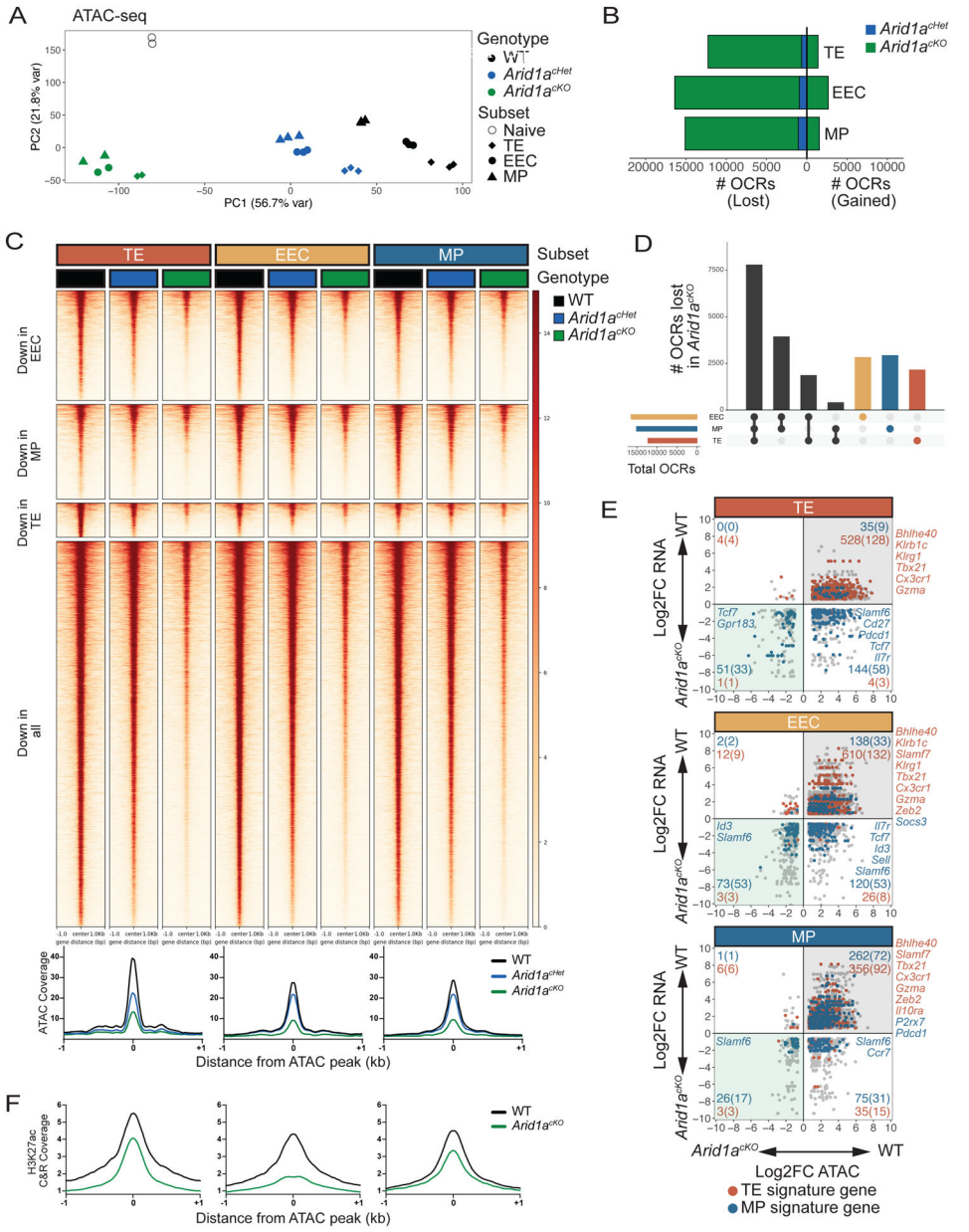

Fig 4. ARID1A-dependent OCRs in d8 MP, EEC, and TE cells are largely shared across subsets.

WT, *Arid1a*^{cKO} and *Arid1a*^{cHet} effector cells were isolated at d8 p.i. and sorted based on expression of TE, EEC and MP markers as defined in Figure 3A and differential OCRs were compared by ATAC-sequencing (2-fold change, adjusted p value<0.05, Benjamini-Hochberg). (A) Principal component analysis plot of ATAC-seq from WT, *Arid1a*^{cHet}, and *Arid1a*^{cKO} subsets at d8 post-infection. (B) Number of OCRs lost and gained in *Arid1a*^{cKO} and *Arid1a*^{cHet} subsets relative to WT cells. (C-D) ATAC-seq signal heatmaps of WT, *Arid1a*^{cHet}, and *Arid1a*^{cKO} d8 subsets. OCRs are clustered by whether they are lost in the *Arid1a*^{cKO} relative to WT cells in individual subsets or lost in all three subsets (C) and UpSet plot shows the number of shared and subset-specific OCRs lost in *Arid1a*^{cKO} subsets relative to WT cells (D). (E) Gene expression and paired chromatin accessibility

of annotated OCRs in *Arid1a*^{cKO} and WT d8 subsets. TE- and MP-signature genes are highlighted in blue and red, respectively. (F) H3K27ac CUT&RUN signal coverage centered on ARID1A-dependent ATAC-seq peaks in WT vs. *Arid1a*^{cKO} cells TE, EEC, and MP cells.

Author Manuscript Author Manuscript Author Manuscript Author Manuscript

Author Manuscript Author Manuscript Author Manuscript Author Manuscript

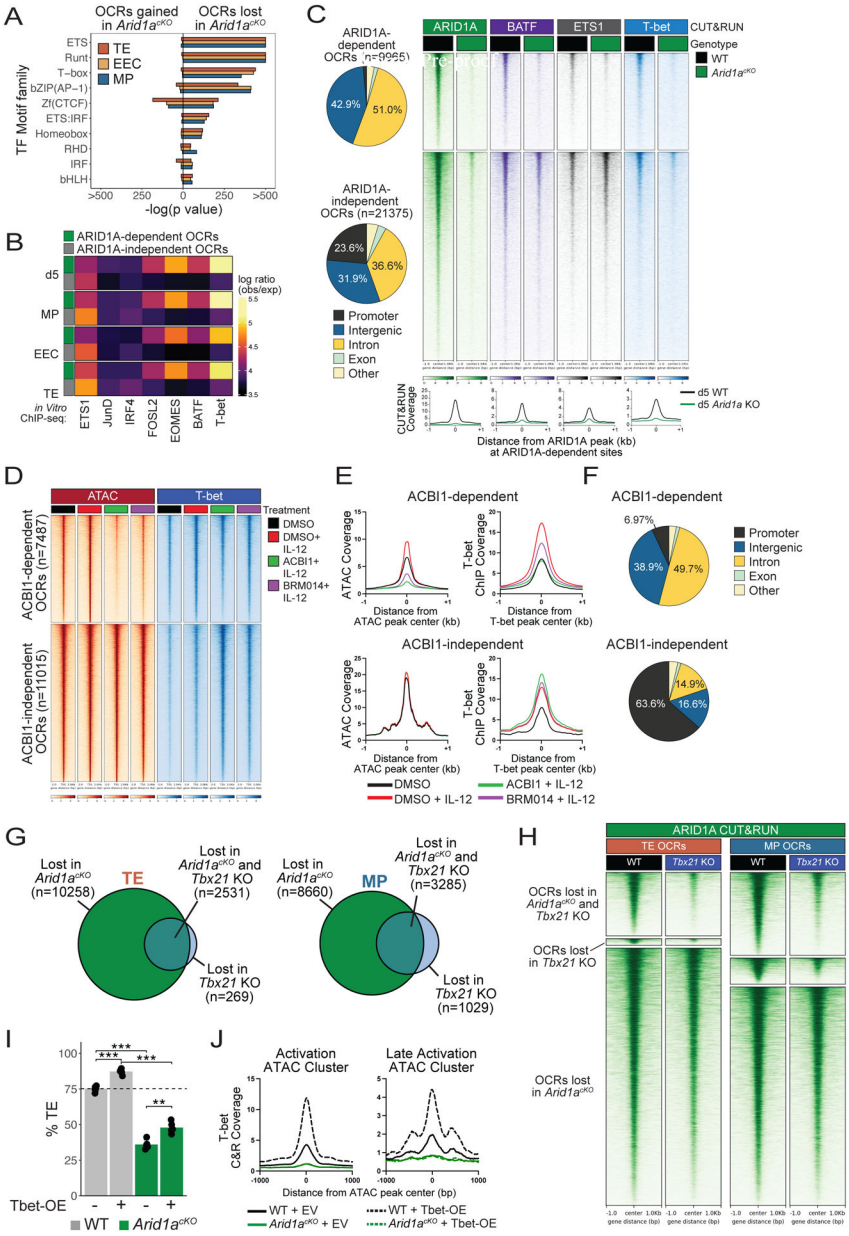

Fig 5. cBAF is required for targeting of T-bet to enhancers in effector CD8$^+$ T cells.

(A-B) As described in Figure 4, OCRs (2-fold change, adjusted p value<0.05, Benjamini-Hochberg) lost in *Arid1a*^{cKO} d5 effector cells or d8 TE, EEC, and MP subsets relative to WT cells were analyzed for enrichment of predicted TF motifs (A) or TF binding signals (observed/expected) of indicated TFs from public ChIP-seq datasets (GSE192390) in ARID1A-dependent (green) and - independent (gray) OCRs (B). (C) Genomic annotations and CUT&RUN signal heatmaps of ARID1A, BATF, ETS1, and T-bet at ARID1A-dependent or -independent OCRs from WT and *Arid1a*^{cKO} effector P14 CD8$^+$ T cells d5 post-infection. (D-F) CD8$^+$ T cells were activated *in vitro* for 48hrs and then treated with DMSO (black, red), ACBI1 (green) or BRM014 (purple) for 4 hours, and then treated with IL-12 (red, green, purple) for 2 hours, and analyzed for changes in ATAC-seq and T-bet

Author Manuscript Author Manuscript Author Manuscript Author Manuscript

binding by ChIP-seq. Signal coverage heatmaps of ATAC-seq and T-bet ChIP-seq (D) and histograms measuring chromatin accessibility (E) are shown. (F) Genomic annotations of ACBI1-dependent and -independent ATAC-seq OCRs. (G) Overlap of OCRs lost relative to WT (2-fold change, adjusted p value<0.05, Benjamini-Hochberg) in *Arid1a*^{cKO} or *Tbx21* KO TE and MP cells. (H) ARID1A CUT&RUN signal heatmap in WT or *Tbx21* KO effector cells at d5 p.i. Signal is centered on ARID1A- or Tbet-dependent OCR peaks identified in (G). (I) Retroviral overexpression of T-bet fails to rescue TE formation in *Arid1a*^{cKO} cells at d8 p.i. (J) T-bet CUT&RUN signal coverage histograms at Activation and Late Activation OCRs in WT or *Arid1a*^{cKO} cells transduced with either empty vector (EV) or T-bet overexpression (Tbet-OE) retrovirus at d5 p.i.*p<0.05, **p<0.005, ***p<0.0005.

Author Manuscript Author Manuscript Author Manuscript Author Manuscript

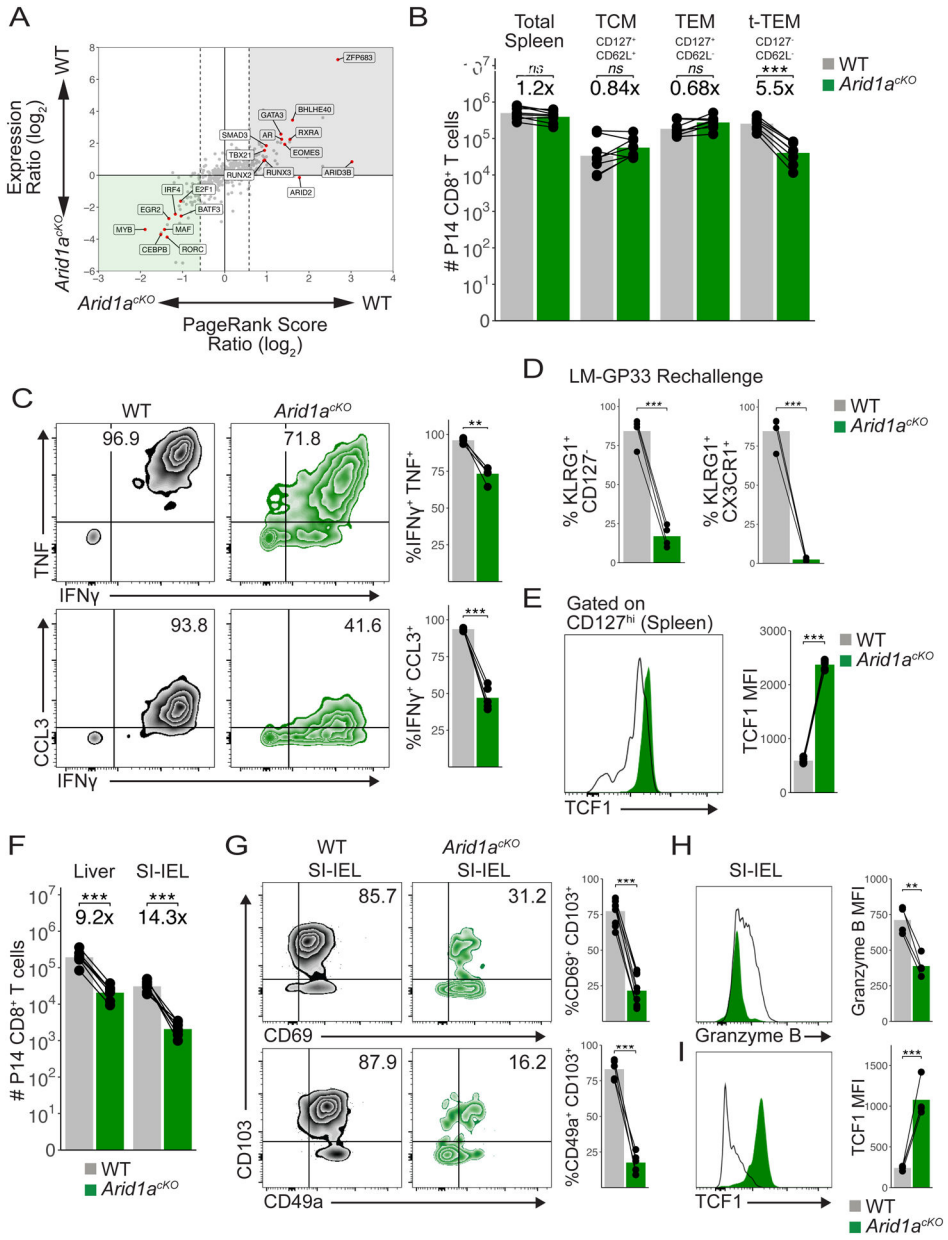

Fig 6. ARID1A is critical for Trm formation.

(A) PageRank and mRNA expression analysis of *Arid1a*^{cKO} and WT MP cells from d8 p.i. (B) Absolute numbers of WT (n=8) and *Arid1a*^{cKO} (n=8) P14 splenic memory cells at d30-d60 p.i. (C) Representative cytokine production in WT (n=4) and *Arid1a*^{cKO} (n=4) memory P14 cells in the spleen at d60 p.i. Mean frequency of IFNg^{+}TNF^{+} (top) and IFNg^{+}CCL3^{+} (bottom) populations are shown. (D) Frequency of KLRG1^{+}CD127^{-} or KLRG1^{+}CX$_3$CR1^{+} secondary effector cells 8d p.i. following LM-GP33 infection in mice that previously received CD127^{+} WT and *Arid1a*^{cKO} LCMV memory P14 cells. (E) TCF1 staining in WT and *Arid1a*^{cKO} CD127^{hi} spleen memory cells at d50 p.i. (F) Absolute numbers of WT and *Arid1a*^{cKO} P14 cells in the liver (n=7) and SI-IEL (n=7) at d50-d60 p.i. (G) Representative flow cytometry plots of WT and *Arid1a*^{cKO} P14 SI-IELs at d60 p.i. Mean frequency of

Author Manuscript Author Manuscript Author Manuscript Author Manuscript

$CD69^+CD103^+$ (top) and $CD49a^+CD103^+$ (bottom) populations are shown. Granzyme B (H) and TCF1 (I) staining in WT and *Arid1a*^{cKO} P14 SI-IELs at d60 p.i. Paired t-test; *p<0.05, **p<0.005, ***p<0.0005.

Author Manuscript Author Manuscript Author Manuscript Author Manuscript

REAGENT or RESOURCE	SOURCE	IDENTIFIER
Antibodies		
BUV737 CD8a	BD	Cat#612759; RRID: AB_2870090
BV421 CD8a	BioLegend	Cat#100738; RRID: AB_11204079
BV605 CD44	BD	Cat#563058; RRID: AB_2737979
BUV395 Thy1.1	BD	Cat#563804; RRID: AB_2632398
BUV496 Thy1.2	BD	Cat#741046; RRID: AB_2870661
PE CD127	BioLegend	Cat#135010; RRID: AB_1937251
PE-Cy7 KLRG1	Invitrogen	Cat#25-5893-82; RRID: AB_1518768
PerCP-Cy5.5 CX3CR1	BioLegend	Cat#149010; RRID: AB_2564494
BUV395 CXCR3	BD	Cat#745689; RRID AB_2743174
BV711 CD49a	BD	Cat#564863: RRID: AB_2738987
BUV737 CD69	BD	Cat#564684; RRID: AB_2738891
BUV395 CD103	BD	Cat#740238; RRID: AB_2739985
BV480 Va2	BD	Cat#746615; RRID: AB_2743895
R718 TCRb	BD	Cat#567299
PE Tbet	BioLegend	Cat#644810; RRID: AB_2200542
PE-Cy7 Eomes	Invitrogen	Cat#25-4875-82; RRID: AB_2573454
AF647 Tcf1	Cell Signaling Technology	Cat#6709S
ARID1A	Abcam	Cat#ab182561
BV421 IFNg	BioLegend	Cat#505830; RRID: AB_2563105
PE-Cy7 TNF	BioLegend	Cat#506324; RRID: AB_2256076
APC CCL3	R&D Systems	Cat#IC450A
PE IL-2	BioLegend	Cat#503808; RRID: AB_315302
PE-Cy7 Granzyme B	Biolegend	Cat#372214; RRID: AB_2728381
PE Granzyme A	ThermoFisher Scientific	Cat#17-5831-82; RRID: AB_2573228
eBioscience™ Fixable Viability Dye eFluor™ 780	ThermoFisher Scientific	Cat#65-0865-14
CellTrace Violet	ThermoFisher Scientific	Cat#C34557
DAPI	BD	Cat#564907
H3K27ac	Abcam	Cat#4729
H3K27me3	Cell Signaling Technology	Cat#9733S
ARID1A	Cell Signaling Technology	Cat#12354S
BATF	Brookwood Biomed	Cat#4003
Tbet	Cell Signaling Technology	Cat#97135S
ETS1	Cell Signaling Technology	Cat#14069
Purified NA/LE Hamster anti-Mouse CD3e	BD	Cat#567114
Purified Hamster anti-Mouse CD28	BD	Cat#553295; RRID: AB_394764
Bacterial and virus strains		
LCMV Armstrong	Kaech and Ahmed, 2001	NA

Author Manuscript Author Manuscript Author Manuscript Author Manuscript

REAGENT or RESOURCE	SOURCE	IDENTIFIER
Listeria monocytogenes GP33-41	Ananda Goldrath	NA
Chemicals, peptides, and recombinant proteins		
GP33-41 peptide	GenScript	Cat#RP20091
Recombinant Murine IL-12p70	R&D Systems	Cat#419-ML-010
Recombinant Murine IL-2	PEPROTECH	Cat# 212-12
Recombinant Murine IL-18	R&D Systems	Cat#9139-IL-010
ACBI1	opnMe	NA
BRM014	MedChemExpress	Cat#HY-119374
Brefeldin A	BioLegend	Cat#420601
ACK Lysing Buffer	VWR	Cat#10128-804
eBioscience Foxp3/Transcription factor staining buffer set	ThermoFisher Scientific	Cat#00-5523-00
eBioscience 10X Permeabilization buffer	ThermoFisher Scientific	Cat#00-8333-56
Cytofix/Cytoperm	BD	Cat#554714
RPMI 1640 Medium	GIBCO	Cat#21875034
Fetal bovine serum	Sigma-Aldrich	Cat#F0804
L-Glutamine	GIBCO	Cat#25030081
2-Mercaptoethanol	GIBCO	Cat#21985023
Penicillin-streptomycin	Invitrogen	Cat#15140148
Collegenase D	Sigma-Aldrich	Cat#11088882001
DnaseI	Sigma-Aldrich	Cat#DN25-5G
HBSS	GIBCO	Cat#14025092
Dithioerythritol	EMD Millipore	Cat#233152
1M HEPES	ThermoFisher Scientific	Cat#15630080
Alt-R S.p. Cas9 Nuclease V3	IDT	Cat#1081059
pA/G-MNase	Epicypher	Cat#14-1048
Critical commercial assays		
P3 Primary Cell 4D X Kit S	Lonza	V4XP-3032
Deposited data		
Raw and analyzed data	This paper	GEO: GSE228381
Experimental models: Organisms/strains		
Mouse: granzyme-B-Cre	The Jackson Laboratory	JAX: 003734
Mouse: C57BL/6J	The Jackson Laboratory	JAX: 000664
Mouse: Tg(TcrLCMV)327Sdz (P14)	Pircher et al., 1989	MGI: 2665105
Mouse: Arid1atm1.1Mag	Chandler et al., 2015	MGI: 5708705
Mouse: Tbx21 KO	Szabo et al., 2002	JAX: 004648
Oligonucleotides		
Recombinant DNA		

Author Manuscript
Author Manuscript
Author Manuscript
Author Manuscript

REAGENT or RESOURCE	SOURCE	IDENTIFIER
MIGR1-Tbet	Joshi et al., 2007	NA
Software and algorithms		
STAR	Dobin et al, 2013	https://github.com/alexdobin/STAR
bwa-mem2	Vasimuddin et al., 2019	https://github.com/bwa-mem2/bwa-mem2
Homer	Heinz et al., 2010	http://homer.ucsd.edu/homer/
DESeq2	Love et al., 2014	https://bioconductor.org/packages/release/bioc/html/DESeq2.html
ggplot2		https://cran.r-proiect.org/web/packages/ggplot2/index.html
deepTools	Ramírez et al., 2016	https://github.com/deeptools/deepTools/
fgsea		https://github.com/ctlab/fgsea